University Abdou Moumouni - Niamey

Doctoral Research Program - Climate Change and Energy (DRP-CCE)

Republic of Niger

SPONSORED BY THE

INTERNATIONAL MASTER'S PROGRAM IN RENEWABLE ENERGY AND GREEN HYDROGEN

SPECIALITY: PHOTOVOLTAICS FOR GREEN HYDROGEN TECHNOLOGY

MASTER'S THESIS

Topic:

SIMULATIONS OF PHOTOLUMINESCENCE TRANSIENTS IN PEROVSKITE SOLAR CELLS

Presented by: **Kouroumlakiwé YOMA** on 27/09/2023

Exam Committee Members:

Chair: Prof. Modou Fall, University Cheikh Anta Diop-Senegal

Examinator: Dr. Karimoun Massalatchi Illyassou, University Abdou Moumouni-Niger

Main Supervisors: Prof. Thomas Kirchartz, Forschungszentrum Jülich-Germany

Prof. Uwe Rau, Forschungszentrum Jülich-Germany

Local Supervisors: Ass. Prof. Moussa Mounkaila Saley, University Abdou Moumouni-Niger

Dr. Abdou Latif Bonkaney, University Abdou Moumouni-Niger

Academic year 2022-2023

Declaration

I hereby declare that this master's thesis titled "Simulations of Photoluminescence Transients in Perovskite Solar Cells" has been carried out by myself. The information derived from the literature has been duly acknowledged in the dissertation and a list of references has been provided. This project work is submitted in partial fulfillment of the requirements for the award of the degree of Master of Photovoltaics for Green Hydrogen Technology.

Kouroumlakiwé YOMA 27th September 2023

This thesis was written at the Research Centre Jülich, Institute of Energy and Climate Research, Photovoltaics (IEK-5)

Dedication

I dedicate this master's degree to my mother MINZA Maguizani, my wonderful brothers, lovely cousins, and friends.

Acknowledgments

I would like to take this opportunity to express my profound gratitude to all those who helped me in one way or the other in conducting research and pursuing my degree.

First and foremost, I would like to thank the Federal Ministry of Education and Research, BMBF especially Prof. Rovekamp, and the West African Science Service Centre on Climate Change and Adapted Land Use, WASCAL for granting me the scholarship to conduct this master's degree.

Next, I would like to thank the research center Jülich, FZJ in Germany where I have conducted my research work especially the Director of the Institute of Photovoltaics and Climate Research IEK5, Prof. Rau Uwe, his team, and administration.

I would also like to express my gratitude to my main research advisors Prof. Thomas Kirchartz, Tobias Rudolph, and Prof. Uwe Rau who have helped me a lot from the beginning of my research work. Without their cooperation and helpful suggestions, completing my research and study was impossible. The doors of their offices were always open whenever I ran into trouble or had a question about my research. Grateful to Prof. Thomas Kirchartz for teaching me his scientific and esthetic rigor. I express my profound gratitude to Tobias Rudolph who always assisted me whenever I needed help, remotely during weekends, and with whom I built a strong relationship. I would like to thank also my co-supervisors, the Scientific Coordinator of WASCAL Niger, Assoc. Prof. Moussa Mounkaila Saley, and Dr. Abdou Latif Bonkaney from Abdou Moumouni University (UAM) for their support, wise advice, and the opportunity to learn things professionally.

I thank the president of the University Abdou Moumouni for hosting me during this program. My special thanks to the director of WASCAL Niger Prof. Adamou Rabani and his team.

I want to express my profound gratitude to the coordinator of the Green Hydrogen program at UAM in Niger Dr. Abdoulkadri Ayouba Mahamane for his friendly and supportive method to motivate me to look for perfection. He always had time for me whenever I ran to him and his wise feedback helped me greatly.

My special thanks to the members of the organic photovoltaic group of IEK5, the group in which I conducted the research. Their support and feedback helped a lot in pursuing my research and improving my work. Special thanks to Chris Dreessen for his support.

Finally, I would like to thank the defense committee for their time and insightful feedback.

Abstract

Perovskite solar cell technology has attracted enormous interest and attention from the research community in recent decades as one of the most promising photovoltaic technologies for future energy generation. This attention is partly due to the continuous increase in the power conversion efficiency of perovskite solar cells, which is approaching that of crystalline silicon technology, the ease of processing the materials, the availability of materials, and the low cost of manufacturing processes. However, the performance of perovskite solar cells is hampered by some charge carrier mechanisms and loss processes within the solar cell, thus hindering the large-scale development of perovskite solar cells.

This work aims to simulate photoluminescence transients in complete perovskite solar cells to understand and gain insight into charge carrier dynamics in perovskite solar cells and different recombination mechanisms, as well as the effects of some material parameters on photoluminescence transients. Therefore, numerical simulations were carried out on a complete perovskite solar cell after excitation by a laser pulse by applying some key assumptions to the proposed model. The thesis explores the approach of a numerical model based on time-dependent derivative triple-coupled ordinary differential equations describing the kinetics of carriers within a complete perovskite solar cell using MATLAB software.

To verify the reliability and accuracy of the numerical approach proposed in this work, experimental measurements of transient photoluminescence from a fabricated complete perovskite solar cell were performed. The results were compared with the SETFOS software to determine the correlation between experimental data and simulations.

Keywords: Perovskite Solar Cells, Photoluminescence Transients, Simulations, Carrier Dynamics.

Résumé

Au cours des dernières décennies, la technologie des cellules solaires à pérovskite a suscité un intérêt et une attention considérables de la part de la communauté des chercheurs, qui la considèrent comme l'une des technologies photovoltaïques les plus prometteuses pour la production d'énergie à l'avenir. Cette attention est en partie due à l'augmentation continue du rendement de conversion de puissance des cellules solaires à pérovskite, qui se rapproche de celui de la technologie du silicium cristallin, à la facilité de traitement des matériaux, à la disponibilité des matériaux et au faible coût des processus de fabrication. Toutefois, les performances des cellules solaires à pérovskite sont entravées par certains mécanismes de porteurs de charge et processus de perte au sein de la cellule solaire, ce qui freine le développement à grande échelle des cellules solaires à pérovskite.

Ce travail vise à simuler les transitoires de photoluminescence dans des cellules solaires complètes à pérovskites afin de comprendre la dynamique des porteurs de charges dans les cellules solaires à pérovskites et les différents mécanismes de recombinaison, ainsi que les effets de certains paramètres des matériaux sur les transitoires de photoluminescence. Dans cette logique, des simulations numériques ont donc été réalisées sur une cellule solaire à pérovskite complète après excitation par une impulsion laser en appliquant certaines hypothèses clés au modèle proposé. La thèse explore l'approche d'un modèle numérique basé sur des équations différentielles ordinaires triplement couplées et dépendantes du temps, décrivant la cinétique des porteurs de charges dans une cellule solaire complète à pérovskite à l'aide du logiciel MATLAB.

Pour vérifier la fiabilité et la précision de l'approche numérique proposée dans ce travail, des mesures expérimentales de la photoluminescence transitoire d'une cellule solaire complète à pérovskite fabriquée ont été réalisées. Les résultats ont été comparés avec le logiciel SETFOS pour déterminer la corrélation entre les données expérimentales et les simulations.

Mots clés: Cellules solaires à pérovskite, transitoires de photoluminescence, simulations, dynamique des porteurs de charges.

Abbreviations and Symbols

AM 1.5: Air Mass under Standard Solar Spectrum

BCP: Bathocuproine

C60: Fullerene

CCD: Charge-Coupled Device

EPBT: Energy Pay-Back Time

ETL: Electron Transport Layer

FTO: Fluorine-doped Tin Oxide

Gt: Gigatonnes

HLI: High-Level Injection

HTL: Hole Transport Layer

ITO: Indium Tin Oxide

LED: Light-Emitting Diode

LLI: Low-Level Injection

LS: Large Signal

MPP Maximum power point

Mtoe: Million Tons of oil equivalent

nip: Negative-intrinsic-positive

ODE: Ordinary Differential Equation

PCE: Power Conversion Efficiency

pin: Positive-intrinsic-negative

PL : Photoluminescence

PSC: Perovskite Solar Cell

QFLS: Quasi-Fermi Level Splitting

SCAPS-1D: Solar Cell Capacitance Simulator, one-dimensional

Spiro-OMeTAD: 2,2',7,7'-tetrakis-(N, N-di-4-methoxyphenylamino)-9,9'-spirobifluorene

SQ: Shockley-Queisser

SRH: Shockley-Read-Hall

TCAD: Technology Computed-Aided Design

TrPL: Transient Photoluminescence

UV: Ultraviolet

C_{area} Capacitance per area

$C_{\mathrm{co,n}}$ Capacitance of the n-type contact

$C_{\mathrm{co,p}}$ Capacitance of the p-type contact

C_{n} Auger recombination coefficient for electrons

C_{p} Auger recombination coefficient for holes

D_{n} Diffusion constant for electrons

D_{p} Diffusion constant for holes

E_{C} Energy level of the conduction band

E_{F} Energy of the Fermi level

E_{Fn} Energy of the quasi-Fermi level for electrons

E_{Fp} Energy of the quasi-Fermi level for holes

E_{g} Band gap energy

E_{t} Energy level of a trap

E_{V} Energy level of the valence band

J_{ext} Extraction current density

J_{inj} Injection current density

J_{MPP} Current density at the maximum power point

J_{ph}	Photogenerated current density
J_{rad}	Radiative current density
J_{rec}	Recombination current density
J_{sc}	Short-circuit current density
J_{SRH}	Shockley-Read-Hall current density
N_{C}	Effective density of states in the conduction band
N_{V}	Effective density of states in the valence band
P_{max}	Maximum attainable power density of a solar cell
P_{sun}	Power density of the solar spectrum
R_{Aug}	Auger recombination rate
R_{rad}	Radiative recombination rate
R_{SRH}	Shockley-Read-Hall recombination rate
V_{ext}	External voltage
V_{int}	Internal voltage $\Delta E_{\mathrm{F}} = qV_{\mathrm{int}}$
V_{MPP}	Voltage at the maximum power point
V_{n}	External voltage which decreases over the n-type contact
V_{OC}	Open-circuit voltage
V_{p}	External voltage which decreases over the p-type contact
e_{n}	Emission coefficient for electrons of a trap in SRH recombination
e_{p}	Emission coefficient for holes of a trap in SRH recombination
k_{rad}	Radiative recombination coefficient
n_{Q}	Charge per volume induced on the capacitor
r_{A}	Ionic radius of molecule or atom in crystal position A
r_{B}	Ionic radius of molecule or atom in crystal position B

r_x	Ionic radius of molecule or atom in crystal position X
C	Capacitance
d	Thickness
F	Electric field
FF	Fill factor
G	Generation rate
h	Planck constant: 4.1357×10^{-15}eVs
J	Current density
k	Boltzmann constant
m	Charge density on the contact
n	Electron density
n_i	Intrinsic charge carrier concentration
n_{id}	Ideality factor
p	Hole density
q	Elementary charge: 1.6022×10^{-19}C
R	Recombination rate
t	Time, also Goldschmidt tolerance factor
T	Temperature
V	Voltage
x	position

Greek symbols

ΔE_F	Fermi-level splitting
β_n	Capture coefficient for electrons of a trap in Shockley-Read-Hall
β_p	Capture coefficient for holes of a trap in Shockley-Read-Hall

μ_{n}	Electron mobility
μ_{p}	Hole mobility
τ_{cell}	Decay time of a perovskite solar cell
τ_{film}	Decay time of a pure film
$\tau_{\mathrm{SRH}}^{\mathrm{eff}}$	Effective Shockley-Read-Hall recombination lifetime
τ_{n}	Electron lifetime in the Shockley-Read-Hall model
τ_{p}	Hole lifetime in the Shockley-Read-Hall model
Δn	Excess electron density
Δp	Excess hole density
η	Energy conversion efficiency
τ	Charge carrier lifetime
υ	Photon frequency

List of Figures

List of Tables

Table of Contents

1. Introduction

1.1 Background

Technological progress in science and medicine over the last century has led to significant global population increase. The population has increased exponentially in the twentieth century, rising from 1.65 billion to 6 billion people throughout this century [1]. This global population is still increasing, and unlikely to stabilize over the century. There is an 80% chance that the current global population of 7.2 billion people will rise to between 9.6 and 12.3 billion people in 2100 [2]. This growth in world population as a result of technological improvements has led to an increase in energy demand and consumption, as well as the expenditure of resources. Between 1995 and 2019, the amount of energy used worldwide increased rapidly, from 8,588.9 million tons of oil equivalent (Mtoe) to 14,907.24 Mtoe [3], [4]. Globally, fossil fuels have been used for centuries to meet the exponential energy demand. The use of fossil fuels to produce energy has brought about some issues related to pollutants such as carbon dioxide, methane, and nitrous oxide. In 2021, energy combustion and industrial activities contributed to 36.3 gigatonnes (Gt) of the world's carbon dioxide emissions [5]. Environmental pollution and climate change are issues caused by the world's energy production model since the industrial revolution, which is based on fossil fuels [6].

To reduce the negative effects of climate change, it is crucial to drastically reduce greenhouse gas emissions by reducing the energy generation by fossil fuels. Thus, the world needs sustainable and less damaging production energy sources and renewables. Various types of renewable energy sources, such as solar, wind, hydropower, geothermal, and biomass energy are available. Among renewable energy sources, photovoltaic solar energy technology stands out as one of the most promising sectors, involving the use of photovoltaic panels to capture solar energy and convert it into electricity [7].

Indeed, there are a variety of photovoltaic cell technologies categorized based on materials used, technology maturity, and processes used in manufacturing the cells. These cell technologies are the crystalline silicon technologies that comprise both the simple crystalline and multi-crystalline forms, thin film cell technologies, and organic photovoltaic technologies. Crystalline silicon technology is a large-scale developed technology, whereas organic photovoltaic technology is still in demonstration and development [7].

Among the emerging photovoltaic technologies, the perovskite solar cell (PSC) technology is promising for the future of energy. Owing to their rapid increase in efficiency, variety of

applications, outstanding light-harvesting properties combined with low manufacturing costs, and the simplicity of processing, perovskites and optoelectronic devices have received a great deal of interest [8]–[10] and exhibit efficiency levels that are over 25%, which are approaching the efficiency of crystalline silicon solar cells [11]. In addition, compared with the crystalline form of silicon, perovskite solar cell technology has a lower manufacturing temperature [12], which reduces the required energy. In terms of energy pay-back time (EPBT), which is the time required for an energy system to generate the energy used during its construction and decommissioning phases, including raw material processing, perovskite solar cells have the shortest energy pay-back time among all photovoltaic technologies [13], which is an indicator of the energy performance of this technology.

While perovskite solar cell (PSC) technology is promising for the energy future, PSCs technology development is hindered by some efficiency and performance loss processes within solar cells. As a result of these loss processes, the open-circuit voltages, and efficiencies are lower under specific lighting conditions [14] and frequently include the fill factor and the short-circuit current [15]. Any solar cell technology, including perovskites, suffers from non-radiative recombination as one of the primary loss processes [14]. Consequently, the performance of perovskite solar cells is limited by these decay recombination processes, which compete with the radiative-free carrier recombination within the cell [8]. Furthermore, the long-term stability of perovskite solar cells is another challenge hindering the large-scale development of this technology. From this perspective, studying and understanding the operating processes of PSCs as well as the recombination processes to identify losses within the perovskite solar cells are crucial for further efficiency improvements.

1.2 Justification and Problem Statement

Transient Photoluminescence (TrPL) on perovskite samples is mostly used on pure films which makes easy the interpretation of the data and measured Photoluminescence (PL). However, the presence of contacts in complete perovskite solar cells, which adds an extra effect, charging and discharging effect, makes it more difficult and challenging to understand and interpret charge carrier kinetics in devices. The effect of contact capacitance (i.e., charging and discharging effects) influences the density of the charge carriers in the perovskite layer, as well as the measured Photoluminescence and decay time.

1.3 Research Questions

How can simple analytical solutions be used to extract the key performance-limiting parameters in complete perovskite solar cells (PSCs)?

How do changes in material properties affect the transient photoluminescence kinetics in perovskite solar cells?

1.4 Objectives of the Thesis

The scope of this thesis is to use TrPL measurements and numerical simulations to understand and analyze the effect of contact capacitance on the charge carrier density in the absorber, that is, the perovskite layer, the measured Photoluminescence transients, and the decay time in fully assembled perovskite solar cells. By analyzing the decay time and photoluminescence plots, recombination losses can be minimized by optimizing the device parameters and properties to improve the performance. Furthermore, this thesis aims to gain insight into the injection, extraction, and recombination of charge carrier mechanisms in perovskite solar cells and extract the thickness d of the absorber over the exchange velocity S_{exc} (d/S_{exc}) time constant ratio for the increase and decrease in charge carrier densities in the absorber from TrPL measurements. TrPL is widely used in pure films and layer stacks but is rarely used in devices. To the best of our knowledge, TrPL in full devices has not yet been studied in the context of numerical simulations. The specific objectives of this thesis are:

1. Use TrPL on a complete perovskite solar cell to consider the charging and discharging effect.
2. Simulate the kinetics of charge decay in typical-time domain measurements.
3. Extract time constant d/S_{exc} for the rise and decrease of charges in the absorber layer

1.5 Structure of the Thesis

The structure of this thesis is presented below. This thesis is divided into four chapters. Chapter 2 outlines the basic and necessary information useful for understanding the content of the work. First, we discuss perovskite solar cell technology. Subsequently, we introduce charge carrier generation and recombination processes in perovskite solar cells and transient photoluminescence as a technique to monitor the kinetics of charge carriers in PSCs. Finally, the photovoltaic performance of a solar cell and the Shockley-Queisser model with different assumptions applied to the model are discussed.

In Chapter 3, we introduce the materials, methods, and simulations used in performing the measurements. we first describe the transient photoluminescence measurement and the setup and then the model used in simulations.

Chapter 4 presents the main results obtained from the measurements and simulations and discusses these findings.

Finally, in session 5, we present the conclusion about the work done and the outlook on perovskite solar cell technology.

Chapter 2: Fundamentals

This chapter provides the necessary understanding and knowledge of perovskite solar cell technology, solar cells in general, and transient photoluminescence (TrPL) to follow the thesis. First, PSCs technology, device architecture, and evolution as an emerging photovoltaic material are presented. Furthermore, the generation and different recombination processes in semiconductors are discussed and explained. As a method to quantify recombination and extraction, transient photoluminescence (TrPL) is introduced and the theory to understand data is discussed. Subsequently, we discuss the photovoltaic performance and some defining parameters. Finally, we explain the Shockley-Queisser model and compare it with a real solar cell.

2.1 Perovskite Solar Cells

2.1.1 Crystal Structure of Perovskite

High-efficiency, easily processed, inexpensive, and readily available materials are essential for solar cell technology [16]. Perovskite solar cells are not only efficient in converting solar energy to electricity but are also easy to fabricate. Therefore, much research has been conducted worldwide to improve the efficiency of perovskite solar cells. The term "perovskite" does not refer only to the crystal structure of semiconducting materials used to make perovskite solar cells but a whole group of materials that crystallize in the chemical formula ABX_3 with A representing an organic or inorganic cation (e.g., methylammonium) and B a metal cation (typically Pb^{2+}), and X, the halide anion (typically I^- and/or Br^-) that coordinates with B to form a BX_6 octahedron (see Fig. 2.1). The name perovskite was given to the mineral $C_aT_iO_3$ (calcium titanate) that was discovered by the German mineralogist Gustav Rose in the Ural Mountains, in honor of the Russian Count, Lev A. Perovski [17]. The production of materials with distinctive semiconducting properties is made possible by the abundance of many organic and metallic ions, which can combine to form perovskite structures [17]. The ratio of ionic dimensions that the perovskite architecture can tolerate is given by the Goldschmidt tolerance factor *t* [18]. This tolerance factor defines the limitations of the possible variations in the perovskite composition and is expressed as

$$t = \frac{r_A + r_B}{\sqrt{2}(r_B + r_X)}, \tag{2.1}$$

where *r* is the radius of the effective ion dimensions of the respective indexed sites. The majority of organic and inorganic perovskite compounds have tolerance factors in the range of $t \approx 0.8$ -1.1[17]. However, the perovskite crystallizes in an ideal cubic structure if this

tolerance factor equals 1. The change in the tolerance factor can result in remarkably diverse electronic properties of perovskites.

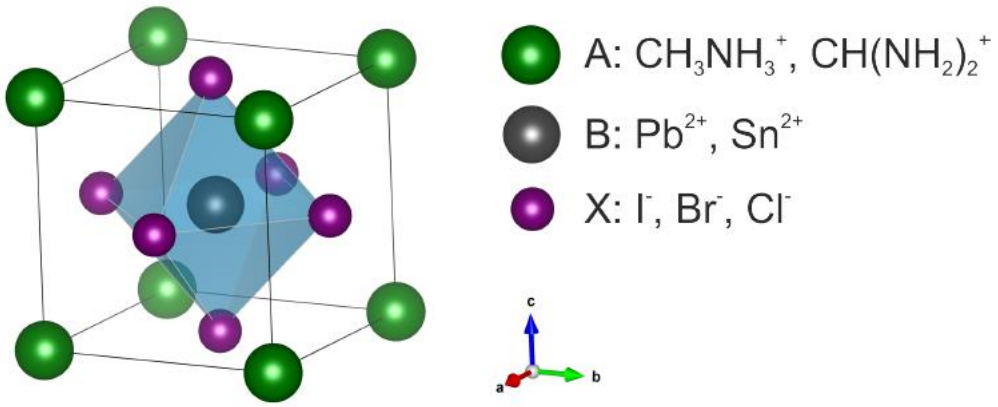

Figure 2.1: Illustration of cubic organic-inorganic perovskite unit cell with the structure ABX3 [19].

2.1.2 Perovskite Solar Cell's Evolution

Before its use in solar cell applications, D. Weber was the first to describe the synthesis of methylammonium lead halide perovskites in 1978 [20]. A few years later, Mitzi et al. developed the first electronic devices by researching charge transport processes in organic-inorganic perovskites in the 1990s [21], [22]. In 2009, perovskites were first used as absorber materials inside dye-sensitized solar cells, resulting in power conversion efficiency (PCE) of up to 3.8% by the research team of Miyasaka [23]. In this device, the perovskite functioned as a thin light sensitizer, covering the mesoporous titanium dioxide scaffold (TiO_2). In 2012, two groundbreaking studies showed that halide perovskites not only have extraordinary light absorption properties but also exceptional conducting properties [24], [25]. These two studies with reported power conversion efficiencies of 10.9% and 9.7% spurred a significant increase in the number of studies being conducted in the field on a global scale. Figure 2.2 shows the evolution of record efficiencies of some solar cell technologies over the years. Perovskite solar cell technology shows the steepest increase in power conversion efficiency in the range 2010-2015. Although research on perovskite solar cells has started for only a few years, the efficiency has significantly improved, indicating that perovskite is a promising material in photovoltaics.

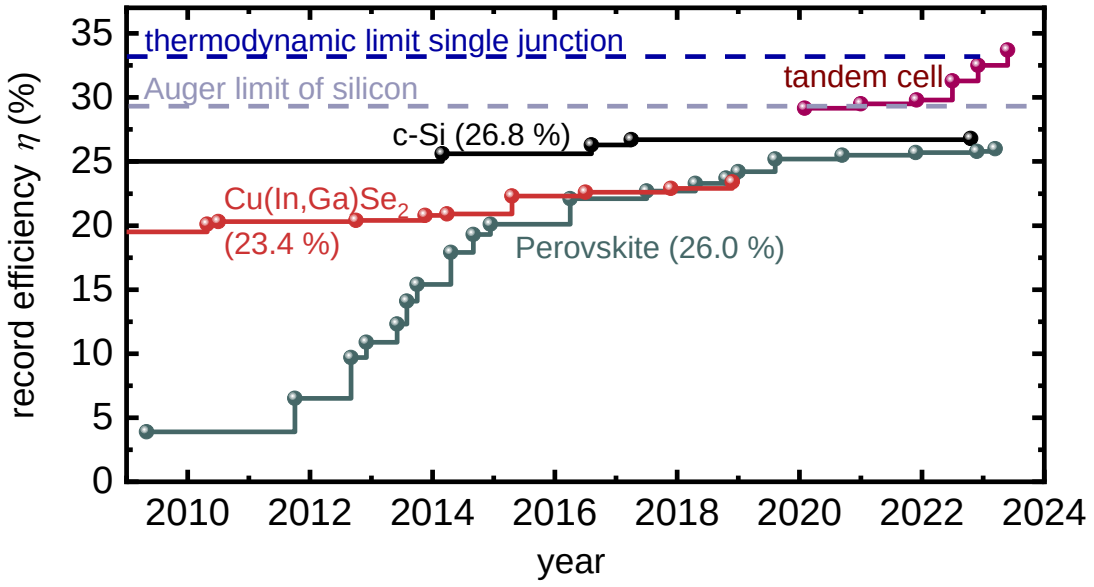

Figure 2.2: Illustration of perovskite solar cell's efficiency evolution over years. Adapted from the research-cell efficiency chart published by the National Renewable Energy Laboratory (NREL) [26].

2.1.3 Transport Layers in Perovskite Solar Cells

Perovskite solar cells are made up of charge transport layers, an electron transport layer (ETL), and a hole transport layer (HTL), which sandwich the absorber layer on both sides and are crucial for the stability and performance of PSCs. A typical Perovskite solar cell is a combination of five layers (see Figure 2.3 (a) and (b)). These parts are transparent conductive electrode that consists of fluorine-doped tin oxide (FTO) or indium tin oxide (ITO), an n-type electron transport layer, a perovskite absorbing layer, a p-type hole transport layer, and a noble metal electrode. The transport layers should meet some requirements for efficient perovskite solar cells. Pathak et al. for instance, showed that for an efficient perovskite solar cell, the electron transport layer must have a good energy alignment for effective charge transfer and hole blocking, high electron mobility, high stability and transmittance, and simple processing and low cost [27]. Titanium dioxide or titania (TiO_2) is commonly used in PSCs as ETL however, recently great attention has attracted the community of researchers towards tin oxide (SnO_2) as a potential substitute ETL for PSCs [28]. Spiro-OMeTAD is mostly used as the HTL in PSCs.

Depending on whether the electron transport layer (ETL) or the hole transport layer (HTL) is deposited first, perovskite solar cells are manufactured in one of two ways [29]. These two cell architectures are nip-type (negative-intrinsic-positive) known as "standard architecture" and

pin-type (positive-intrinsic-negative) known as “inverted architecture” and illustrated in Figures 2.3 (a) and (b). In the nip-type, an n-type conducting material, such as the often-used titania, is placed on the bottom, followed by a layer of intrinsic perovskite, and on top, a p-type organic semiconductor while in the pin-type, it starts at the bottom with a p-type selective contact, followed by a layer of intrinsic perovskite and an n-type organic semiconductor on top. Both architectural designs can achieve eminent power conversion efficiencies of over 20–22% [30]. However, nip-type PSCs have shown maximum efficiencies for single-junction cells and open-circuit voltages [19], [31]. Thus, the efficiencies of pin-type PSCs were much lower than those of nip-type PSCs. This disparity might result from a lower open-circuit voltage (V_{OC}) for pin-type PSCs because of the unsuitable doping state of the perovskite near its n-type interface, which causes a higher non-radiative recombination rate [32].

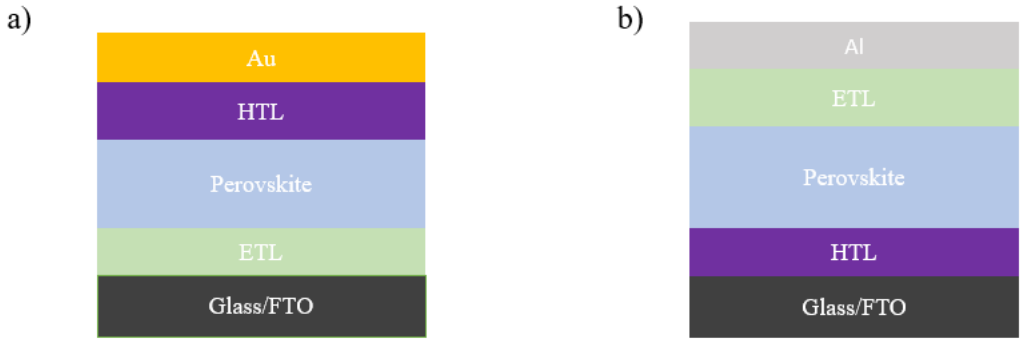

Figure 2.3: Illustration of two types of perovskite solar cells (a) nip-type PSCs (standard architecture) and (b) pin-type PSCs (inverted architecture).

Research studies on perovskites have focused on other applications, such as optoelectronic applications, semiconductor diodes, and light-emitting diodes (LEDs) [33], owing to the high luminescence efficiencies of perovskites [34].

2.2 Generation and Recombination

Every microscopic process has an inverse process that balances it in thermal equilibrium. This principle, known as detailed balance, is important for understanding the limitations of different solar cells in terms of their photovoltaic performance [19]. Recombination is the process through which electron-hole pairs are produced in reverse [34]. The recombination processes play a key role in this work because photoluminescence, which consists of measuring photons emitted from a semiconductor after being released by radiative recombination, is based on these

processes. There are two types of charge-carrier recombination processes in semiconductors: radiative and non-radiative recombination.

2.2.1 Radiative Recombination

From a thermodynamic point of view, radiative recombination, known as inverse absorption, is an unavoidable process [19]. Radiative recombination requires one electron and one hole to get involved in the recombination process. After being internally produced by radiative recombination, the photon can either be released from the sample or reabsorbed by the sample itself before it can leave the sample. In direct semiconductors, recombination via radiation is the predominant process [34]. The electron and hole carrier densities *n* and *p,* respectively, determine how quickly the charge carriers recombine. The radiative recombination rate is described by

$$R_{\mathrm{rad}} = k_{\mathrm{rad}}\,(np - n_i^2), \tag{2.2}$$

where k_{rad} is the radiative recombination constant, *n* and *p* are the carrier concentrations of electrons and holes respectively, and n_{i}, the intrinsic charge carrier density of a semiconductor.

It is important to note that the rate of radiative recombination of an absorber in a solar cell is typically not the rate that will be measurable from the outside. The likelihood that photons will be reabsorbed and form new electron-hole pairs and the likelihood that they will be parasitically absorbed in one of the contact layers both affect the probability that photons will be released from the absorber [34]. This results in loss mechanisms that have an impact on the photoluminescence process.

2.2.2 Non-Radiative Recombination

Non-radiative recombination, as well as radiative recombination, takes place in optoelectronic materials. In Contrast to radiative recombination, which causes a photon to be created and possibly radiated from the absorber, non-radiative recombination involves the deposition of energy that is stored in charge carriers as phonons into the crystal lattice. Although radiative recombination cannot be avoided because of thermodynamics, one of the main objectives of solar cell design is to decrease non-radiative recombination [34] because any solar cell technology, including perovskites, suffers from non-radiative recombination as one of the primary loss processes [14]. There are fundamentally three types of non-radiative recombination: Shockley-Read-Hall recombination, Auger recombination, and non-radiative band-to-band recombination. However, non-radiative band-to-band recombination of electron-hole pairs might, in theory, operate through multi-phonon emission non-radiatively and are

unlikely to occur, particularly with materials with high band gaps and relatively low phonon energy [19]. In this work, attention will be paid to the Shockley-Read-Hall recombination.

2.2.2.1 Shockley-Read-Hall Recombination

Shockey-Read-Hall recombination is a non-radiative recombination process that is one of the most well-known recombination mechanisms in semiconductors. This recombination mechanism occurs at traps, such as impurities, defects in the structure of the semiconductor, or foreign atoms in the device. The only cause of free carrier recombination in the device under application-relevant conditions is trap-assisted and surface recombination [8]. The rate of recombination is also dependent on the defect types, shallow or deep defects, and the position of the defect in the bandgap. These defects influence the device performance through recombination. Yuan et al. studied the influence of defects on the performance of a device and showed that shallow traps are less problematic for device performance than deep traps with given Shockley-Read-Hall lifetimes [15]. The traps may be used to hold charge carriers and produce phonons. This charge carrier capture is highly dependent on the energetic distance between the location of the charge carriers and the trap in the semiconductor. Recombination via localized, singly charged states in the band gap through multi-phonon emission is described by the statistics of Shockley-Read-Hall mechanisms. As these states frequently result from impurity atoms and defects, a reduced Shockley-Read-Hall recombination rate indicates a relatively pure, defect-free, and highly crystalline semiconductor material [19].

The Shockley-Read-Hall recombination rate was defined under various assumptions and considerations. Under the assumption that recombination is dominated by Shockley-Read-Hall recombination through defects, whether shallow or deep defects, the recombination rate is given by

$$R_{\mathrm{SRH}} = N_{\mathrm{t}}\beta_{\mathrm{n}}\beta_{\mathrm{p}}\frac{np-n_i^2}{n\beta_{\mathrm{n}}+p\beta_{\mathrm{p}}+e_{\mathrm{n}}e_{\mathrm{p}}}, \tag{2.3}$$

where N_t is the trap density, β_{n} , β_{p} are the capture coefficients of electrons and holes respectively, $e_{\mathrm{n}}, e_{\mathrm{p}}$ are the emission coefficients of electrons and holes respectively.

The emission coefficients are given as

$$e_{\mathrm{n}} = \beta_{\mathrm{n}}N_{\mathrm{C}}\exp\left(\frac{E_{\mathrm{t}}-E_{\mathrm{c}}}{kT}\right) = \beta_{\mathrm{n}}n_1 \tag{2.4}$$

$$e_{\mathrm{p}} = \beta_{\mathrm{p}}N_{\mathrm{V}}\exp\left(\frac{E_{\mathrm{V}}-E_{\mathrm{t}}}{kT}\right) = \beta_{\mathrm{p}}p_1 , \tag{2.5}$$

where N_C and N_V are the effective density of states for conduction and valence band respectively, E_t is the trap energy and

$$n_1 = N_c \exp[(E_t - E_c) / kT] \tag{2.6}$$

and

$$p_1 = N_V \exp[(E_V - E_t) / kT] \tag{2.7}$$

are abbreviations of unit concentration that include information on charge carrier detrapping. Furthermore, k is the Boltzmann constant, and T the temperature.

Under the assumption that $n = p$ and $n \gg n_i$, the SRH recombination rate can be expressed as

$$R_{SRH} = \frac{n^2}{(n+n_1)\tau_p + (n+p_1)\tau_n}, \tag{2.8}$$

where $\tau_n = 1 / \beta_n N_t$ and $\tau_p = 1 / \beta_p N_t$ are respectively the electron and hole lifetime.

In addition, under the assumption that the defect resides in the middle of the band gap, hence $n \gg n_1 = p_1$ and we assume also that we have $\tau = \tau_n + \tau_p$, high-level injection (HLI). Therefore, the SRH recombination rate is further simplified and expressed as

$$R_{SRH} = \frac{n}{\tau_n + \tau_p} = \frac{n}{\tau}. \tag{2.9}$$

2.2.2.2 Auger Recombination

Auger recombination is another non-radiative recombination mechanism that occurs in semiconductors. This process involves three charge carriers. During the recombination process, electrons and holes recombine; however, the energy that results from this recombination is not released in the form of a photon but is rather transferred to a third electron or hole. This third charge carrier thermalizes back to the band edge after being activated deep within the band it was previously in, releasing its energy as a phonon to the lattice. The recombination rate of the Auger process is given by

$$R_{Aug} = \left(C_n n + C_p p\right)(np - n_i^2), \tag{2.10}$$

where C_n and C_p are the Auger recombination coefficients for electrons and holes respectively.

Figure 2.4 illustrates the abovementioned recombination processes in semiconductors.

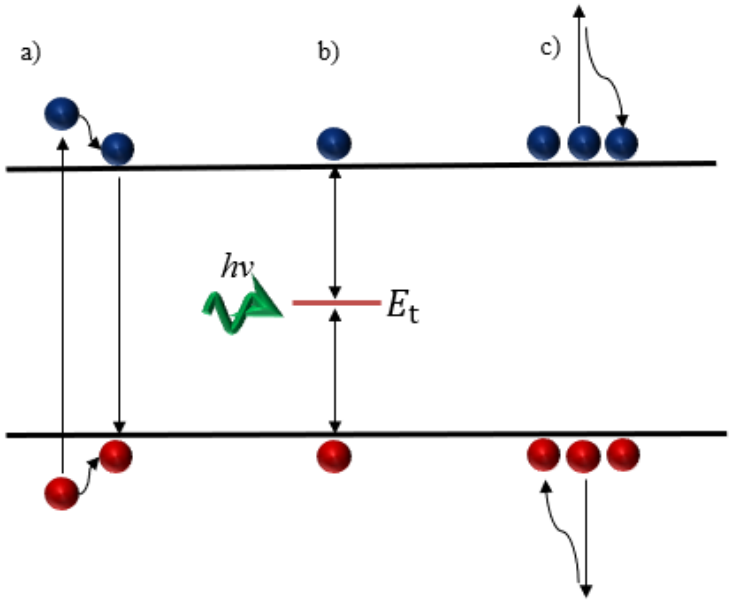

Figure 2.4: Illustration of recombination processes in semiconductors. (a) Generation, thermalization, and radiative recombination. (b) Shockley-Read-Hall recombination through a trap level at the energy E_t. (c) Auger recombination.

2.3 Transient Photoluminescence

Transient Photoluminescence (TrPL) experiments have been widely used in the area of perovskite photovoltaics to study the key recombination parameters. The kinetics of charge transfer and/or recombination on nanosecond timescales can be revealed using TrPL [35]. TrPL measures a transient response to a short laser pulse stimulation or excitation and aims to determine in pure films and in complete solar cell devices recombination parameters. Transient Photoluminescence measurements can provide quantitative data on the recombination processes in layer stacks [35]. It detects the photoluminescence that is produced by radiative recombination between a population of electrons and holes in the absorber material as a function of the delay time after the laser pulse [36]. The excitation conditions used in PL measurements have a significant impact on the recombination characteristics of semiconductors [35]. Additionally, the product *np* of the concentrations of electrons and holes affects how much photoluminescence (PL) is emitted from the semiconductor (i.e., PL~np). To quantify the amount of photoluminescence emitted by a semiconductor or solar cell, it is important to calculate the electron and hole concentrations as a function of external voltage. This is possible by applying the continuity equations that account for electrons

$$\frac{dn}{dt} = G_{\mathrm{ext}}(\mathrm{x},\mathrm{t}) + G_{\mathrm{int}}(x,t,n,p) - R(x,t,n,p) + D_{\mathrm{n}}\frac{d^2n(x,t)}{d\mathrm{x}^2} + F\mu_{\mathrm{n}}\frac{dn(x,\mathrm{t})}{dx} \qquad (2.11)$$

and holes

$$\frac{dp}{dt} = G_{\text{ext}}(x,t) + G_{\text{int}}(x,t,n,p) - R(x,t,n,p) + D_{\text{p}}\frac{d^2p(x,t)}{dx^2} - F\mu_{\text{p}}\frac{dp(x,t)}{dx}, \quad (2.12)$$

where x is the position normal to the cell surface, t the time, n and p the electrons and holes concentrations respectively, $D_{\text{n/p}} = \mu_{\text{n/p}}kT/q$ the diffusion constants for electrons and holes, kT/q the thermal voltage (25.8 mV at room temperature), F the electric field, $\mu_{\text{n/p}}$ the electrons and holes mobilities, R is the recombination rate, G_{ext} the generation rate for electron-hole pairs as a result of external illumination and G_{int} the internal generation as a result of photons absorption generated by the radiative recombination within the cell itself.

Diffusion and drift, which control the flow of electrons and holes, are the final two terms in equations (2.11) and (2.12). It is important to note that the kinetics of trapping and de-trapping, which may occur in the event of shallow defects present in the semiconductor, were not considered in these equations. Furthermore, thermal emission from shallow traps, especially for materials with extremely short minority carrier lifetimes, considerably influences the PL transients [35]. This effect is considerably lower in perovskite solar cells, which have much longer carrier lifetimes.

Continuity equations are often reduced in practice, which makes it possible to derive analytical solutions for the electron and hole concentrations in a steady-state or transient experiment. If the terms for the diffusion and drift currents are neglected, analytical solutions to the continuity equation can be employed [15]. Hence, with the assumption that the system is without spatial gradients of electron and hole concentrations or the electrostatic potential and that compared to the photogenerated carrier density, the density of doping is negligible (high-level injection situation), the continuity equations can be further simplified and written as

$$\frac{d\Delta n}{dt} = \frac{d\Delta p}{dt} = G_{\text{ext}}(t) + G_{\text{int}}(t,n) - R(t,n), \quad (2.13)$$

where $\Delta n = n - n_{\text{o}}$ and $\Delta p = p - p_{\text{o}}$ are the excess electron density and the excess hole density relative to the density at the equilibrium n_{o} and p_{o} respectively. It is important to bear in mind that if the sample is doped, the doping densities would be included in n_{o} or p_{o}.

In steady state, the ratio $d\Delta n/dt = d\Delta p/dt = 0$. Therefore, the continuity equation is reduced to

$$G_{\text{ext}} + G_{\text{int}}(n) = R(n). \quad (2.14)$$

From equation (2.14), under steady-state conditions, the concentrations of electrons and holes can be obtained, provided that the recombination rate dependence on the charge carrier is

known. The product *np* of electron and hole concentrations determines the amount of light emitted, whereby this product becomes $np = n^2$ in an intrinsic semiconductor [35]. As a result of charge carrier generation, the Fermi level is split into two: one for electrons and one for holes. Quasi-Fermi levels (QFLs) are the usual name for these new Fermi levels in what is typically called quasi-thermal equilibrium. The charge carrier densities are defined as

$$n = N_{\mathrm{C}} \exp\left(\frac{E_{\mathrm{Fn}} - E_{\mathrm{C}}}{kT}\right) \tag{2.15}$$

and

$$p = N_{\mathrm{V}} \exp\left(\frac{E_{\mathrm{V}} - E_{\mathrm{Fp}}}{kT}\right), \tag{2.16}$$

where E_{Fn} and E_{Fp} are the QFLs for electrons and holes, respectively.

The product np of these equations leads to

$$np = N_{\mathrm{C}} N_{\mathrm{V}} \exp\left(\frac{E_{\mathrm{Fn}} - E_{\mathrm{C}}}{kT}\right) \exp\left(\frac{E_{\mathrm{V}} - E_{\mathrm{Fp}}}{kT}\right) = N_{\mathrm{C}} N_{\mathrm{V}} \exp\left(-\frac{E_{\mathrm{g}}}{kT}\right) \exp\left(\frac{\Delta E_{\mathrm{F}}}{kT}\right), \tag{2.17}$$

where ΔE_{F} is the Quasi-Fermi level splitting (QFLS) and relates to a voltage that builds up inside a solar cell's absorber.

Thus, the quasi-Fermi level splitting ΔE_{F} in the absorber layer can be obtained through the photoluminescence flux via

$$\Delta E_{\mathrm{F}} = kT \ln\left(\frac{np}{n_{\mathrm{i}}^2}\right) = kT \ln\left(\frac{n^2}{n_{\mathrm{i}}^2}\right) = 2kT \ln\left(\frac{n}{n_{\mathrm{i}}}\right), \tag{2.18}$$

where $n_{\mathrm{i}}^2 = n_{\mathrm{o}} p_{\mathrm{o}} = N_{\mathrm{C}} N_{\mathrm{V}} \exp\left(-\frac{E_{\mathrm{g}}}{kT}\right)$ and $np = n^2$ (intrinsic semiconductor).

Equation (2.18) shows that the quasi-Fermi level splitting of the luminescent material is measured by the absolute intensity of steady-state photoluminescence. This quasi-Fermi level splitting will be a function of illumination parameters, SRH lifetime, recombination prefactor, and the density of charge carrier at the equilibrium n_{i}, and the band gap E_{g} as well [35]. The benefit of measuring the quasi-Fermi level splitting by photoluminescence purely optically is the ability to determine the maximum open-circuit voltage that a layer or layer stack could deliver in the absence of any additional recombination losses [37], [38].

2.3.1 Injection Characteristics

2.3.1.1 Low-Level Injection

The condition called low-level injection (LLI) of a semiconductor under illumination depends on the doping density and the incoming light intensity. Most of the conventional semiconductor materials used in optoelectronic devices are doped. LLI occurs in a semiconductor when the

majority carrier concentration is higher than the minority carrier concentration, even under of moderate illumination, provided that the doping is sufficiently high. The number of free holes is several orders of magnitude greater than the number of free electrons in an unilluminated p-type semiconductor ($p \gg n$). Let us assume that the semiconductor in LLI is p-type with a doping density N_A. Here, electrons are the minority charge carriers, and holes are the majority charge carriers. We further assume that N_A is much greater than the photo-generated carrier density ($N_A \gg \Delta n = \Delta p$), then $p \approx N_A$, the recombination rate equations (2.2), (2.3), (2.10) and (2.18) in LLI can be simplified as

$$R_{\mathrm{rad}} = k_{\mathrm{rad}}(nN_A - n_i^2) \tag{2.19}$$

$$R_{\mathrm{SRH}} = \frac{\Delta n}{\tau_n} \tag{2.20}$$

$$R_{\mathrm{Aug}} = C_p n N_A^2 \tag{2.21}$$

$$\Delta E_F = kT \ln\left(\frac{n}{n_0}\right). \tag{2.22}$$

Equations (2.19), (2.20), (2.21), and (2.22) show that each of the recombination rates in LLI is linear with respect to the minority carrier density (electrons in this case).

2.3.1.2 High-Level Injection

In contrast to LLI, high-level injection (HLI) is a situation where the concentrations of both free electrons and holes are equal ($n = p$). In other words, the semiconductor in HLI is not doped. Typically, in photoluminescence experiments, lead-halide perovskites act as intrinsic or low-doped semiconductors[35]. In addition to the assumption of $np > n_i^2$, the HLI can simplify the recombination rate equations (2.2), (2.3), (2.10), and (2.18) as well.

$$R_{\mathrm{rad}} = k_{\mathrm{rad}} n^2 \tag{2.23}$$

$$R_{\mathrm{SRH}} = \frac{n}{\tau_n + \tau_p} \tag{2.24}$$

$$R_{\mathrm{Aug}} = (C_p + C_n) n^3 \tag{2.25}$$

$$\Delta E_F = kT \ln\left(\frac{n^2}{n_i^2}\right). \tag{2.26}$$

In contrast to the LLI, the recombination rates depend on the electron density or hole density in different ways. HLI is crucial for understanding the different aspects that will be discussed in perovskite solar cells in this work.

2.4 Photovoltaic Performance

Solar cells are devices that convert the light harvested from the sun into electrical energy. When sunlight strikes the solar cell, the energy of the photons is absorbed by the electrons in the solar cell. These electrons are then excited to a higher energetic state, leaving behind holes and positively charged carriers. At the opposite ends of the solar cell, the charge carriers, electrons, and holes are extracted, producing a current. The conversion of solar radiation into electricity is due to the photovoltaic effect observed for the first time in 1839 by Becquerel [39].

2.4.1 Photovoltaic Parameters

Many parameters define the photovoltaic performance of a solar cell such as power conversion efficiency (η), open-circuit voltage (V_{OC}), the short-circuit current density (J_{SC}), the fill factor (FF). The current density-voltage curve known as $J(V)$ characteristic of a solar cell under illumination conditions provides data on these parameters. Figure 2.5 illustrates an example of this curve.

The V_{OC} is the voltage in the solar cell when the current density $J = 0$ and J_{SC} is the current density that flows when the voltage $V = 0$ (i.e., when the solar cell is short circuited) and is the largest current which may be drawn from a solar cell, η the ratio between the electric power density P_{el} and the power density of incoming light P_{sun}. There is an operating point at which the maximum power is provided, maximum power point (MPP), with corresponding J_{MPP} and V_{MPP} that define the maximum efficiency. The fill factor is defined as

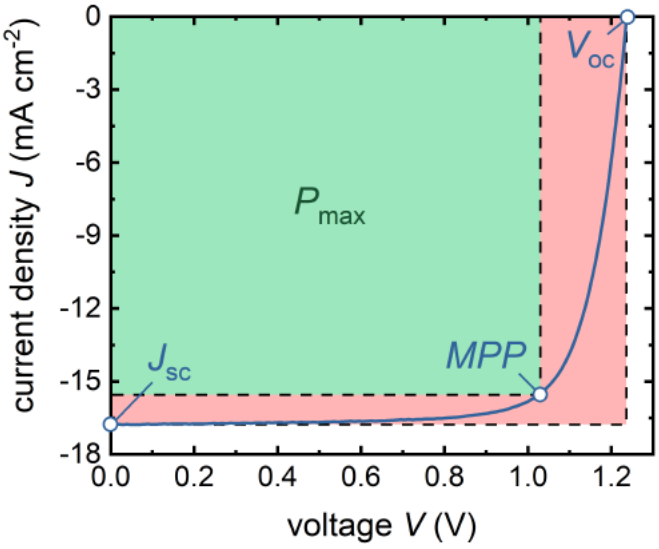

Figure 2.5: Illustration of the current-voltage curve of a solar cell under illumination conditions [34].

$$FF = \frac{J_{\mathrm{MPP}} V_{\mathrm{MPP}}}{J_{\mathrm{SC}} V_{\mathrm{OC}}} \tag{2.27}$$

and is an indicator of the ability of a solar cell to extract charge carriers with minor resistive losses.

The efficiency is defined as

$$\eta = \frac{P_{\max}}{P_{\mathrm{sun}}} = \frac{J_{\mathrm{MPP}} V_{\mathrm{MPP}}}{P_{\mathrm{sun}}} = \frac{J_{\mathrm{SC}} V_{\mathrm{OC}} FF}{P_{\mathrm{sun}}}. \tag{2.28}$$

Equation (2.28) shows that the higher the J_{SC} and V_{OC}, the higher the efficiency of a solar cell.

2.4.2 Diode Equation and Determination of Photovoltaic Parameters

We assume a solar cell as an idealized diode as illustrated in Figure 2.6 and determine the expressions of J_{SC} and V_{OC}. The characteristic curve equation of an ideal solar cell is

$$J = J_{\mathrm{ph}} - J_{\mathrm{o}} \left[\exp\left(\frac{qV}{n_{\mathrm{id}} kT} \right) - 1 \right] \tag{2.29}$$

where J_{ph} is the photocurrent density which is the number of photons absorbed by the solar cell, $\mathrm{J_o}$,the saturation current density, n_{id} the ideality factor (n_{id} equal to one in the ideal case), and q the elementary charge.

If V=0 is applied to Equation 2.29, the exponential term vanishes, and then, $J_{\mathrm{SC}} = J_{\mathrm{ph}}$ (the short-current density is equal to the photocurrent density).

To determine the V_{OC} , J=0 is applied to Equation (2.29), then the open-circuit voltage is

$$V_{\mathrm{OC}} = \frac{n_{\mathrm{id}}\, kT}{q} \ln\left(\frac{J_{\mathrm{ph}}}{J_{\mathrm{o}}} + 1 \right).$$

Since $J_{\mathrm{SC}} = J_{\mathrm{ph}}$ and with very small currents, the value 1 can be neglected compared to $\mathrm{J_{SC}/J_o}$, the expression of the open-circuit voltage is further simplified to

$$V_{\mathrm{OC}} = \frac{n_{\mathrm{id}}\, kT}{q} \ln\left(\frac{J_{\mathrm{SC}}}{J_{\mathrm{o}}} \right).$$

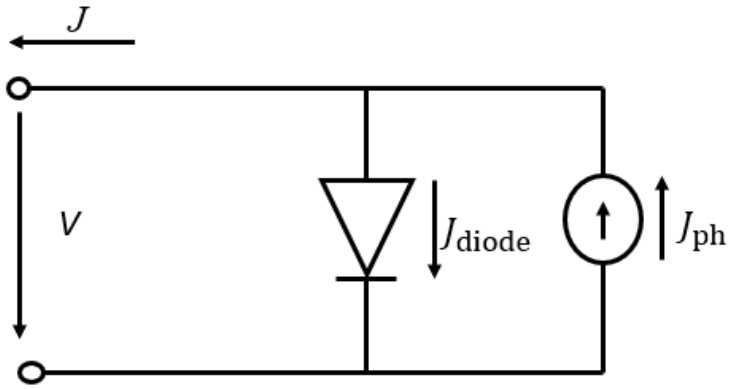

Figure 2.6: Illustration of the diode equivalent circuit of an ideal solar cell

2.5 Shockley-Queisser Model

The Shockley-Queisser (SQ) limit specifies the greatest solar energy conversion efficiency possible for a given material, which serves as a benchmark for evaluating new photovoltaic technology [40]. This SQ model is based on the principle of detailed balance. In 1961, for the first time, William Shockley and Hans-Joachim Queisser reported the maximum conversion efficiency of the p-n junction solar cell illuminated by the sun through the detailed balance principle [41]. The efficiency limit for a perovskite solar cell is about 31 % which approaches the Shockley-Queisser efficiency limit of around 33.5 % under AM1.5 spectrum of sun for a single-junction solar cell reached by gallium arsenide (GaAs) [42]. The SQ model is based on five assumptions that constitute the essence of the model and are important for the understanding of the model. These assumptions are presented below

1. For an ideal solar cell, the highest possible efficiency is reached when there is no non-radiative recombination occurring in the solar cell. This means that there are only two possibilities for an electron-hole pair in the solar cell: either the electron and hole recombine radiatively or they are collected at their respective contacts.
2. For any photon with an energy above the band gap energy ($h\upsilon \geq E_g$) absorbed by the solar cell, there is a generation of one electron-hole pair with a quantum efficiency of 100% while any photon absorbed by the solar cell with an energy below the band gap energy ($h\upsilon < E_g$) will not interact with the solar cell. In other words, the absorptance in this model is a step-function switching from 0 *(*$h\upsilon < E_g$) to 1 ($h\upsilon \geq E_g$). h and υ are Planck constant and frequency respectively.
3. Most of the photons absorbed have a higher energy than the band gap energy; therefore, the excess energy after generating electron-hole pairs is released into the lattice of the

semiconductor in the form of phonons, resulting in the movement of charge carriers at the band edges, as illustrated in Figure 2.7. The third assumption is known as thermalization. This means that in thermal equilibrium with the cell, every electron-hole pair thermalizes to the same average energy. However, this assumption is not the case in real solar cells, where the ambient temperature is much lower than the temperature within the solar cell under illumination conditions, resulting in a drop in solar cell efficiency.

4. Every absorbed photon with $h\nu \geq E_g$ generates exactly one electron-hole pair which is collected at a short circuit.
5. In the absence of resistive losses for the charge carriers in the absorber, the contacts are perfectly selective.

These five assumptions define the ideal solar cell in the SQ model. Based on these assumptions, the reduction in efficiency from an ideal solar cell to a real solar cell is due to three types of energy loss: optical losses (i.e., loss of photons that are not absorbed), thermal losses (i.e., loss of the excess kinetic energy), and electronic losses (i.e. loss by photon emission and isothermal dissipation during carrier collection) [41].

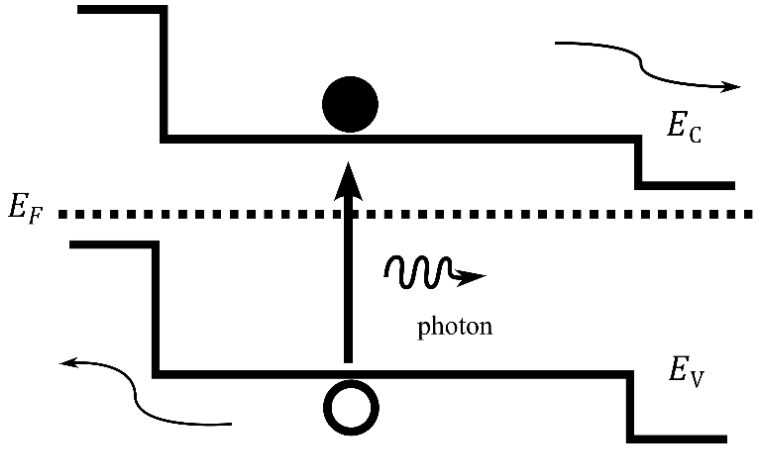

Figure 2.7: Illustration of photovoltaic power conversion of a solar cell.

The power conversion process consists of three steps: light absorption, local thermalization straight after photogeneration, and collection of charges with one more thermalization within the semiconductor and contacts. The photons coming from the source of light generate electron-hole pairs and these charge carriers are collected at the contacts after they have thermalized towards the band edges.

In contrast to what is observed in the Shockley-Queisser model, in a real solar cell, in addition to the non-radiative recombination processes occurring, there are also electrical losses. As illustrated in Figure 2.8, there are series resistance R_s and shunt resistance R_{sh}. The series resistance R_s indicates the ohmic losses at the semiconductor interface and the front contacts of the solar cell while the shunt resistance R_{sh} models the leak currents at the edges of the solar cell and any point where the p-n junction is short-circuited. The characteristic curve equation of a real solar cell is

$$J = J_{ph} - J_o \left[\exp\left(\frac{q(V+JR_s)}{n_{id}kT}\right) - 1\right] - \frac{V+JR_s}{R_{sh}}, \tag{2.30}$$

with $\frac{V+JR_s}{R_{sh}} = J_{sh}$, the shunt current density.

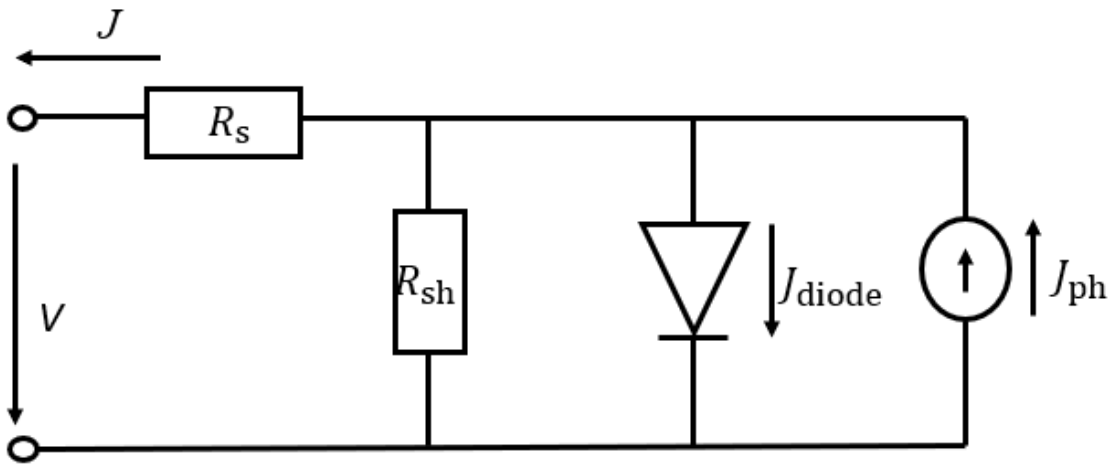

Figure 2.8: Illustration of the diode equivalent circuit of a real solar cell.

Equation 2.30 is reduced to the characteristic curve equation of an ideal solar cell (Equation 2.29) for $R_s = 0$ and $R_{sh} = \infty$. In this case, J_{ph} is not anymore represented by the short-circuit density J_{SC} since they are not equal at V=0.

Chapter 3: Methods and Simulations

In this chapter, the methods and simulations used to perform transient photoluminescence (TrPL) in PSCs are explained and discussed as well as the model. Furthermore, the experimental procedure is introduced and described.

3.1 Numerical Simulations

Numerical simulations in complete perovskite solar cells present many advantages in the research area. Numerical simulations can provide useful information about the kinetics of charge carriers inside the solar cell, the properties of the cell, as well as the key performance limiting mechanisms. To find the best arrangement for perovskite-based solar cells, numerical simulations offer a more affordable option than conducting experiments and make simple the optimization of the design of perovskite solar cells [43]. Numerical simulations can highlight the influence of many device parameters such as the thickness of the absorber, the effective lifetime, trap density and depth, and the capacitance on the performance of the perovskite solar cells [44]. In sum, numerical simulations can help understand the working principle of perovskite solar cells and get insights for further performance improvements of the device.

There are many simulation models and software that are used in perovskite solar cells such as MULTIPHYSICS, SCAPS-1D (Solar Cell Capacitance Simulator, one-dimensional), AMPS (Analysis of Microelectronic and Photonic Structures), and MATLAB. There are also some commercial software such as SETFOS, ASA, and Sentaurus TCAD (Technology Computed-Aided Design) that are used to simulate perovskite solar cells. In this work, we conduct numerical simulations using mainly MATLAB software however, we also use SETFOS to simulate and compare the model.

3.1.1 Justification of the Choice of the Software

Numerical simulations conducted in the work are based on MATLAB software. MATLAB is very popular for simulating perovskite solar cells. The software presents a lot of advantages. The user-friendly interface of MATLAB makes it simple to define the model and simulation input parameters and is highly customizable [45]. The fact that MATLAB is highly customizable helps researchers to write their own scripts and functions to perform specific tasks. In addition, MATLAB offers capabilities for data analysis and visualization, and is simple to link with other programs to carry out more complex simulations. MATLAB uses also an analytical program for numerical simulations in perovskite solar cells [46]. The last but not

the least, MATLAB is very accurate software for performing numerical simulations in perovskite solar cells.

3.1.2 Steps of the Simulations.

The solution to a system of three coupled time-dependent differential equations requires numerical simulations. In this work, the forward problem method is used, which consists of forecasting the characteristics of perovskite solar cells using well-defined and known input parameters and physical model. First, the method defines the device structure with the material properties, subsequently the physical model. Secondly, the method sets the mathematical model to solve the differential equations that describe the kinetics of charge carriers inside the perovskite solar cell. Applying the boundary conditions and assumptions to the mathematical model allows us to solve the differential equations and simulate the characteristics of the perovskite solar cell.

3.2 Model

Below is illustrated the transient methods in the perovskite solar cell.

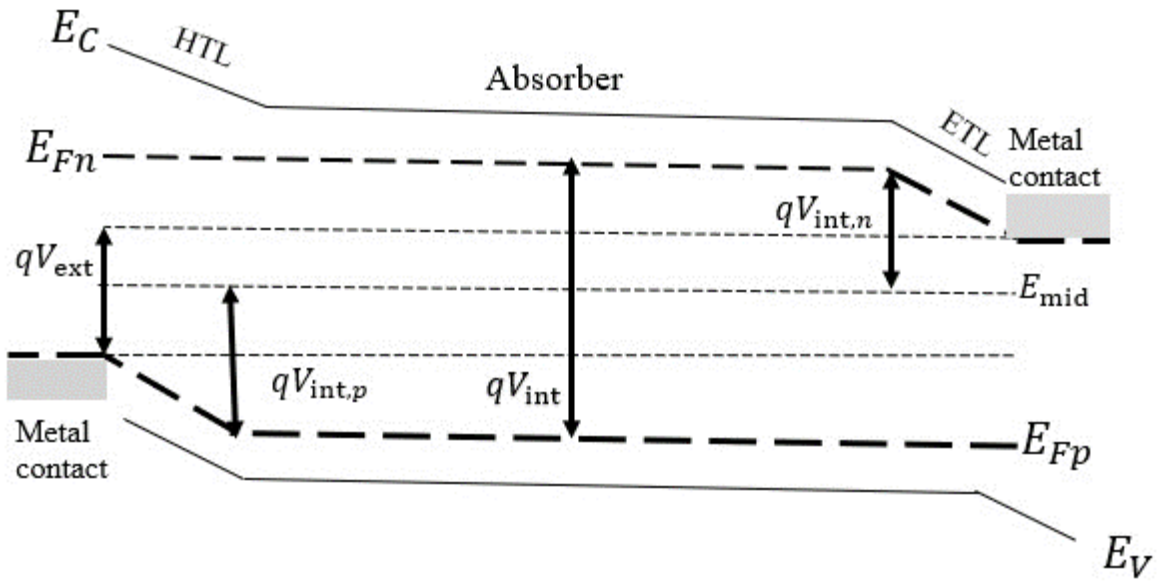

Figure 3.1: Illustration of the model describing the kinetics of charge carriers in the perovskite absorber layer after a laser pulse excitation.

qV_{ext} represents the voltage between the electrodes, V_{int} the internal voltage in the absorber between E_{Fn} and E_{Fp}, the quasi-Fermi level splitting (QFLS) resulting from the splitting of

Fermi-level E_{F} after charge carrier recombination in the absorber, and $V_{\mathrm{int,n}}$ and $V_{\mathrm{int,p}}$ the part of the internal voltage lost at ETL and HTL respectively.

3.2.1 Assumptions in the Model/Boundary Conditions

For simplification purposes of the model, we apply some assumptions to the model to diminish the complexity of numerical methods. These assumptions are below.

1. Any gradient of quasi-Fermi level over the transport layers is neglected during the transient Photoluminescence.
2. The charge transport in the absorber is fast relative to recombination i.e., the movement of charge carriers in the perovskite layer is rapid compared to the rate of recombination.
3. The model is in high-level injection (HLI) i.e., the concentration of both types of charge carriers are present in approximately the same concentrations, $n = p$.
4. Contacts are symmetric i.e., same exchange velocity S_{exc} for the two types of contacts; same capacitance for the two contacts; V_{ext} decreases by an equal amount over the electron and hole contacts.
5. No electrostatic potential drops over the absorber layer i.e., there is no voltage drop across the perovskite absorber layer in the cell.
6. Auger recombination is neglected for simplifying the mathematical model describing the physical processes involved in perovskite solar cells.

3.2.2 Model Description

A complete perovskite solar cell is excited with a laser pulse. After laser excitation, charge carriers are generated in the absorber layer by the absorbed light and subsequently transported to the electrode contacts. However, while charge carriers are immediately generated in the absorber layer and transported to the electrodes after a laser pulse, there is a delay in the build-up of the external voltage due to the capacitance. This delay allows the external voltage V_{ext} , shown in Figure 3.1, to reach its maximum value before it decays. Since the system is symmetric and in high-level injection, the differential equation describing the kinetics of charge carriers n in the absorber is given by [11] and expressed as

$$\frac{\mathrm{d}n}{\mathrm{d}t} = -k_{\mathrm{rad}}n^2 - \frac{n}{\tau_{\mathrm{SRH}}^{\mathrm{eff}}} - \frac{J_{\mathrm{exc}}}{qd}$$

$$= -k_{\mathrm{rad}}n^2 - \frac{n}{\tau_{\mathrm{SRH}}^{\mathrm{eff}}} - \frac{S_{\mathrm{exc}}}{d}\left(n - n_{\mathrm{i}}\exp\left(\frac{qV_{\mathrm{ext}}}{2kT}\right)\right), \tag{3.1}$$

where $\tau_{\mathrm{SRH}}^{\mathrm{eff}}$ is the effective Shockley-Read-Hall recombination lifetime, q the elementary charge, d the thickness of the absorber, S_{exc} the exchange velocity, and J_{exc} the exchange current flowing to or from the electrodes.

The value of the term J_{exc} in Eq. (3.1) is very important in this model. A positive value of the exchange current implies a reduction of the charges in the absorber, while a negative value implies that the charges injected from the electrodes flow back into the absorber through the transport layers. The ratio d/S_{exc} expresses a time constant for the reduction and rise of carrier densities. The motion of electrons between the absorber and the contact on the n-type electrode defines the change of excess charge density σ_{n} per area and is expressed as

$$\frac{\mathrm{d}\sigma_{\mathrm{n}}}{\mathrm{dt}} = qS_{\mathrm{exc}}\left[n - n_{\mathrm{i}}\exp\left(\frac{qV_{\mathrm{ext}}}{2kT}\right)\right]. \tag{3.2}$$

The charge density σ_{n} expresses the external voltage which decreases over the n-type contact as $V_{\mathrm{n}} = \sigma_{\mathrm{n}}/C_{\mathrm{co,n}}$ where $C_{\mathrm{co,n}}$ represents the capacitance of the n-type contact. To simplify the model, we assumed that contacts are symmetric. Therefore, in the model, the capacitance is the same over the two contacts $C_{\mathrm{co,n}} = C_{\mathrm{co,p}}$ and the voltages $V_{\mathrm{n}} = V_{\mathrm{p}}$ over the electron and hole contact as well. From these abovementioned simplifications, the external voltage V_{ext} is expressed as $V_{\mathrm{ext}} = V_{\mathrm{n}} + V_{\mathrm{p}} = 2V_{\mathrm{n}}$ and the total electrical capacitance $1/C_{el} = 1/C_{\mathrm{co,n}} + 1/C_{\mathrm{co,p}} = 2/C_{\mathrm{co,n}}$.The time derivative equation for the external voltage V_{ext} is described as

$$\frac{\mathrm{d}V_{\mathrm{ext}}}{dt} = \frac{q\mathrm{S}_{\mathrm{exc}}}{C_{\mathrm{el}}}\left(n - n_{\mathrm{i}}\exp\left(\frac{qV_{\mathrm{ext}}}{2kT}\right)\right). \tag{3.3}$$

Eq. (3.1) and (3.3) represent the required system of two coupled differential equations. The variables in these differential equations are carrier density and electrostatic potential. It is possible to express the carrier density as function of the quasi-Fermi level splitting as illustrated in Eq. (2.26) of chapter 2,

$$n(\mathrm{t}) = p(\mathrm{t}) = n_{\mathrm{i}}\exp\left(\frac{\Delta E_{\mathrm{F}}}{2kT}\right) = n_{\mathrm{i}}\exp\left(\frac{qV_{\mathrm{int}}(t)}{2kT}\right), \tag{3.4}$$

where $\Delta E_{\mathrm{F}} = qV_{\mathrm{int}}$. With $\mathrm{d}V_{\mathrm{int}}/\mathrm{d}n = 2kT/(qn)$, the time derivative of the internal voltage is expressed as

$$\frac{\mathrm{d}V_{int}}{dt} = \frac{2kT}{qn(V_{\mathrm{int}})}\left[-k_{\mathrm{rad}}n(V_{\mathrm{int}})^2 - \frac{nV_{\mathrm{int}}}{\tau_{\mathrm{SRH}}^{\mathrm{eff}}} - \frac{S_{\mathrm{exc}}}{d}\left(n(V_{\mathrm{int}}) - n_{\mathrm{i}}\exp\left(\frac{qV_{\mathrm{ext}}}{2kT}\right)\right)\right]. \tag{3.5}$$

Eq. (3.3) and (3.5) combined give a system of two coupled differential equations showing the kinetics of two potentials.

3.2.3 Equations of the Decay Time in a Pure Film and a Complete Perovskite Solar Cell

The decay time refers to the time it takes for the PL signal to decay to its initial value after excitation. The importance of plotting the decay time as a function of the chemical potential is to distinguish between different contributions to the decay time from different carrier mechanisms [14]. The equations expressing the decay time in a complete perovskite solar cell and a pure perovskite film are derived below.

From Eq. 3.1, $\frac{dn}{dt} = -k_{\mathrm{rad}}n^2 - \frac{n}{\tau_{\mathrm{SRH}}^{\mathrm{eff}}} - \frac{S_{\mathrm{exc}}}{d}\left(n - n_{\mathrm{i}}\exp\left(\frac{qV_{\mathrm{ext}}}{2kT}\right)\right)$,

with $\exp\left(\frac{qV_{\mathrm{ext}}}{2kT}\right) = \exp\left(\frac{q^2md}{2C_{\mathrm{area}}kT}\right) = \exp\left(\frac{m}{n_{\mathrm{Q}}}\right)$.

In case where the capacitor is charged, we have

$$n - n_{\mathrm{i}}\exp\left(\frac{qV_{\mathrm{ext}}}{2kT}\right) = 0, \frac{n}{n_{\mathrm{i}}} \approx \exp\left(\frac{m}{n_{\mathrm{Q}}}\right)$$

where m is the charge density on the contact and is much larger than n. In the reinjection approximation, the time derivative of m and n is expressed as

$$\left(\frac{dn}{dt} + \frac{dm}{dt}\right) = -k_{\mathrm{rad}}n^2 - \frac{n}{\tau_{\mathrm{SRH}}^{\mathrm{eff}}},$$

with the time derivative for m expressesd as

$$\frac{dm}{dt} \approx \frac{d}{dt}\left(n_{\mathrm{Q}}\ln\frac{n}{n_{\mathrm{i}}}\right) = \frac{n}{n_{\mathrm{Q}}}\frac{dn}{dt},$$

therefore, $\frac{d}{dt}(n+m) = \left(1 + \frac{n_{\mathrm{Q}}}{n}\right)\frac{d}{dt}n = -k_{\mathrm{rad}}n^2 - \frac{n}{\tau_{\mathrm{SRH}}^{\mathrm{eff}}}$,

thus

$$\tau_{\mathrm{cell,HLI}}^{\mathrm{LS}} = -\frac{n}{dn/dt} = \frac{(n_{\mathrm{Q}}/n)\ +1}{k_{\mathrm{rad}}n + 1/\tau_{\mathrm{SRH}}^{\mathrm{eff}}}, \tag{3.6}$$

and with the approximation that $n_{\mathrm{Q}} \ll n(t)$ (typical case on a pure film),

$$\tau_{\mathrm{film,HLI}}^{\mathrm{LS}} = \frac{1}{k_{\mathrm{rad}}n(t) + 1/\tau_{\mathrm{SRH}}^{\mathrm{eff}}}, \tag{3.7}$$

where $n_{\mathrm{Q}} = 2C_{\mathrm{area}}kT/q^2d$ is the charge per volume induced on the capacitor, $\tau_{\mathrm{SRH}}^{\mathrm{eff}}$ the effective Shockley-Read-Hall lifetime, n the density of charges, k_{rad} the radiative recombination coefficient, C_{area} the capacitance per area, d the thickness of the perovskite layer, k Boltzmann constant, T the temperature, and q the electrical charge. Eq. (3.6) and (3.7) represent the decay time on a complete perovskite solar cell and a pure film respectively.

In addition, the rate currents have been calculated and simulated to describe different mechanisms in perovskite solar cells after a laser pulse. These mechanism rate currents are radiative recombination, Shockley-Read-Hall recombination, extraction and injection respectively expressed as

$$J_{\mathrm{rad}} = k_{\mathrm{rad}}(n^2 - n_i^2), \tag{3.8}$$

$$J_{\mathrm{SRH}} = \frac{n-n_i}{\tau}, \tag{3.9}$$

$$J_{\mathrm{extr}} = \frac{S_{\mathrm{exc}}}{d}\left(n - n_i \exp\left(\frac{qmd}{CkT}\right)\right), \text{ and} \tag{3.10}$$

$$J_{\mathrm{inj}} = -J_{\mathrm{extr}}, \tag{3.11}$$

where m represents the charge carriers on the contact and C the capacitance.

3.2.4 Simulation Methodology

We performed numerical simulations using MATLAB script based on coupled rate equations for transient photoluminescence (TrPL). MATLAB script was developed by Thomas Kirchartz for only large signal based on the script by Lisa Krückemeier, and adapted to complete perovskite solar cell by Uwe Rau. The MATLAB script considers the large signal case, i.e., without bias light, on complete perovskite solar cell devices and solves ordinary differential equations for the charge carrier over time. Different types of ordinary differential equations are used in the MATLAB script. The time derivatives, $\mathrm{d}n/dt$ and $\mathrm{d}p/dt$ for the concentrations of electrons, holes respectively, and occupied defects are included in the equations that I solved for the TrPL numerical simulations.

3.2.5 Mathematical Solver

Ode15s is the mathematical solver I used in this thesis for ordinary differential equations. These differential equations are time derivative equations and define the kinetics of charge carriers in perovskite solar cells. Ode15s integrates a system of differential equations taking into account the initial conditions set in the system from an initial time t_0 to a final time $t_0 + dt$. Electrons

and holes are the variables used in this model. The differential equations describing the kinetics of charge carriers and the defects are stiff differential equations i.e., the solution is changing quickly within a small interval of time and slowly within a large time interval. Therefore, in order to handle these stiff differential equations, the solver ode15s uses a variable order technique that modifies the step size in accordance with the stiffness of the equation.

3.2.6 Input Parameters

In performing numerical simulations, input parameters play a crucial function on the output of the simulations. Some of those input parameters including the perovskite solar cell material parameters are introduced in this section.

3.2.6.1 Material parameters

Material parameters are important in numerical simulations. These parameters include physical properties of the perovskite material such as the energy band gap E_{g}, the density of states N_{C} and N_{V}, the absorber thickness d, the electrode capacitance and much more.

3.2.6.2 Defect states

In numerical simulations of perovskite solar cells, defect states are important input parameters These defect states are used to reveal the dynamics of charge carriers in perovskite solar cells and how they affect different recombination mechanisms within the cell. Most numerical simulations in perovskite solar cells use Shockley-Read-Hall recombination to describe charge carrier recombination currents.

3.2.6.3 Charge carrier lifetime

It is an important input parameter that defines the time charge carriers remain free before they recombine within the solar cell. The longer the lifetime of charge carriers, the more efficient the extraction of charges.

3.2.6.4 Exchange velocity

The exchange velocity is an important input parameter in simulating complete perovskite solar cells. It defines the speed at which charge carriers are transferred between the absorber and contacts in the transport layers.

3.2.6.5 Capacitance

The capacitance is an important parameter in the simulations. It is the parameter that shows the capacity of the device to store and release charge carriers. This parameter is varied in the simulations to illustrate how it affects the transient photoluminescence.

3.3 Transient Photoluminescence Experiment

3.3.1 Description of Transient Photoluminescence Setup

TrPL measurements are used in perovskite solar cells to analyze the recombination loss processes. TrPL setup is shown in Figure 3.2. The setup consists mainly of three different units: the laser unit, the spectrometer unit, and the gated charge-coupled device (CCD) camera unit. The CCD camera used to measure the transient photoluminescence decay is iStar DH720 from Andor Solis.

The UV laser has a wavelength of 343 nm and a repetition rate of either 100 Hz or 1000Hz. To vary the intensity, different OD filters were used, an excitation fluence of 0.16 nJ/cm^2,6.38 nJ/cm^2 and 5.49 nJ/cm^2, with an illuminated spot area of 12.56 cm^2.

A photoluminescence signal is emitted after the excitation of the sample. This PL is proportional to the Fermi-level splitting according to

$$\Delta E_{\mathrm{F}}(t) = \Delta E_{\mathrm{F}}(0) + kT \ln\left(\frac{\phi(t)}{\phi(0)}\right), \tag{3.12}$$

where ϕ represents the photon flux and $\Delta E_{\mathrm{F}}(0) = kT \ln(\Delta n^2(0)/n_i^2)$, the initial Fermi-level splitting determined by the average density Δn of generated electrons and an estimated n_i of $7.83 \times 10^{-8}\mathrm{cm}^{-3}$.

This photoluminescence signal is coupled to the spectrometer. In the spectrometer, the PL signal is diffracted by the grating unit and spectrally dispersed. The spectrally dispersed signal from the sample attached to the spectrometer as shown in Figure 3.2 is subsequently detected by the CCD camera. Photoluminescence is measured as a function of time with the gated CCD camera.

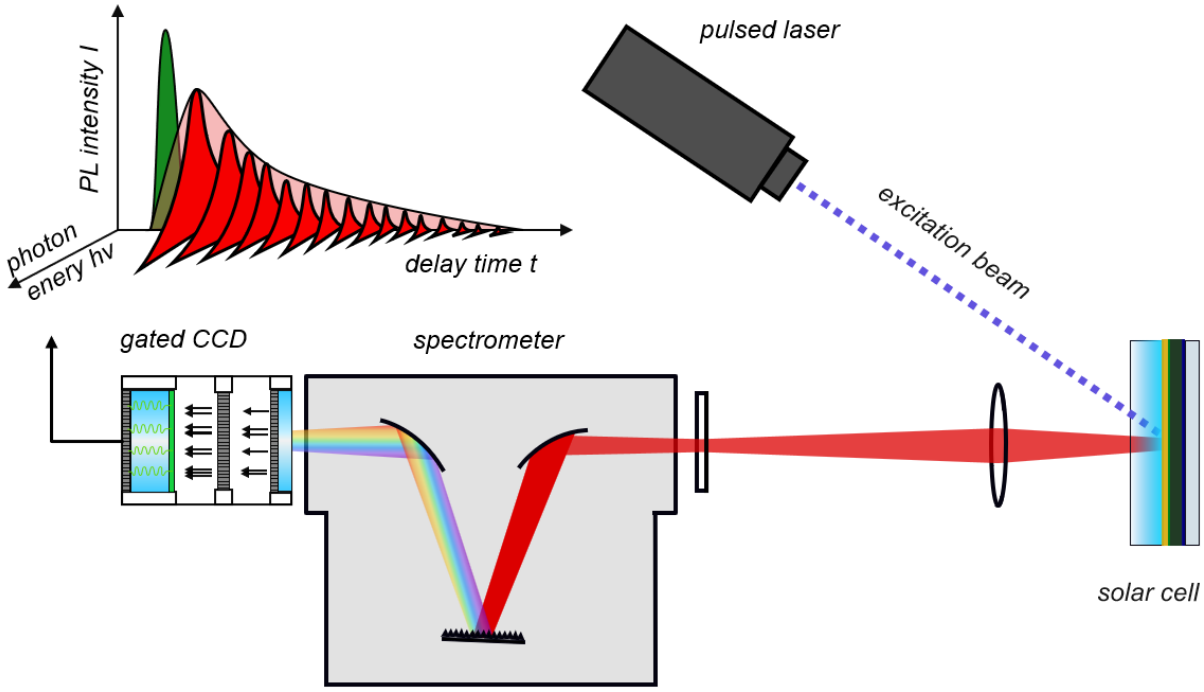

Figure 3.2: Illustration of transient photoluminescence (TrPL) setup. Modified and adapted from [36].

3.3.2 Description of the Experiment

The TrPL measurement consists of different steps that are described below.

Devices were prepared as discussed and described in [47]. The device consists of an ITO, the transparent conductive oxide followed by a mixSAMSPTAA (Poly triaryl amine) coating as a hole contact and transport layer. The absorber is CsFAMAPbI3-xBrx followed by an C60 (fullerene), BCP (bathocuproine) and Ag, the electron transport layer and contact respectively. Table 3.1 shows the device performance characteristics.

Table 3. 1: Parameters of the device used.

Parameters	**Units**	**Values**
Open-Circuit Voltage	V	1.40
Short-Circuit Density	mA/cm^2	19.59
Fill Factor	%	79.08
Power Density	mW/cm^2	17.64
Voltage at MPP	V	0.97
Current Density at MPP	mA/cm^2	18.19

In the measurement, the sample is excited with a laser pulse and then the photoluminescence is measured with a CCD camera as a function of delay time after the laser pulse. A pulsed UV-solid-state laser is used in the experiment as the source of excitation serving as a pump laser for two dye lasers, used for different setups. For the TrPL measurement, we use the UV-laser as an external trigger. For implementing the external triggering, the UV-laser pulse is split into two beams with a beam splitter. One part of the UV-laser pulse after being split into two beams is directed to trigger a diode. The emitted radiation after triggering the diode through an optical fiber impinges on the sample surface and illuminates a spot size.

The sample as a result of the radiative recombination mechanism of the excited charge carriers in the perovskite layer emits a PL signal which is focused on and coupled into the spectrometer as illustrated in Figure 3.2.

The spectrally dispersed signal is then detected by a CCD camera. In the CCD camera, the optical signal is converted first into an electrical signal by a photocathode, amplified by a microchannel plate, back-converted with the help of a phosphor screen, and finally detected by a CCD chip. The spectrum of the PL intensity is then obtained as a function of wavelength.

Time-resolution is obtained by measuring the PL spectra at different delay times, we use the functionality of the intensified CCD camera and a signal of a laser diode as a trigger. The PL is then measured at different times after the excitation pulse by varying the delay time between the trigger signal and acquisition of a spectrum. One can then integrate all recorded spectra over wavelength and plot the photoluminescence intensity as a function of delay time after the laser excitation.

3.4 Software for Data Processing and Analysis

OriginLab is the software mostly used in this work to clean the data obtained from the simulations performed in MATLAB and PYTHON and plot the graphs. OriginLab is the software of choice for scientists and engineers. The software offers a friendly interface for users and is highly customizable with the advantage of connecting with other software such as MATLAB and applications such as Microsoft.

Chapter 4: Results and Discussion

This chapter presents the main findings of this work and the parameters used in experiments and numerical simulations. Furthermore, it discusses and interprets the results obtained and compares them to previous works done in the area. To describe and analyze the kinetics of charge carriers and different mechanism processes in a complete perovskite solar cell, transient photoluminescence simulations were carried out on a complete perovskite solar cell with the presence of contacts as described in section 2.1.3 of the fundamentals.

4.1 Analytical solution comparing a complete perovskite solar cell and a pure perovskite film

In this work, we focus on simulating photoluminescence transients in a complete perovskite solar cell to get insight into various mechanisms happening within the cell rather than simulating on a pure perovskite film that has been subject to various studies so far. In this part, we use the analytical solution to describe the decay of charge carriers in both the complete perovskite solar cell and the pure perovskite film.

The analytical solution of the decay in a complete perovskite cell and the pure perovskite is illustrated in Figure 4.1, plotted from Eq. (3.6) and (3.7). In Figure 4.1(a), the decay time is plotted as a function of the chemical potential $\mu/q = \Delta E_{\mathrm{F}}$ expressed in Eq. 2.18 as

$$\Delta E_{\mathrm{F}} = kT \ln\left(\frac{n^2}{n_i^2}\right).$$

The decay time curve of the pure perovskite film (Fig.4.1, curve in blue) shows two regions: a constant decay time region at low chemical potential or low carrier concentration and the region of exponential (radiative) decrease of the decay time at high chemical potential or high carrier concentration. At low chemical potential, the decay time approaches the effective Shockley-Read-Hall lifetime $\tau_{\mathrm{SRH}}^{\mathrm{eff}} = 2\mu s$. Whereby, at high chemical potential, the exponential decay is dominated by the radiative recombination mechanism. This radiative decay is limited by $1/k_{\mathrm{rad}}n$.

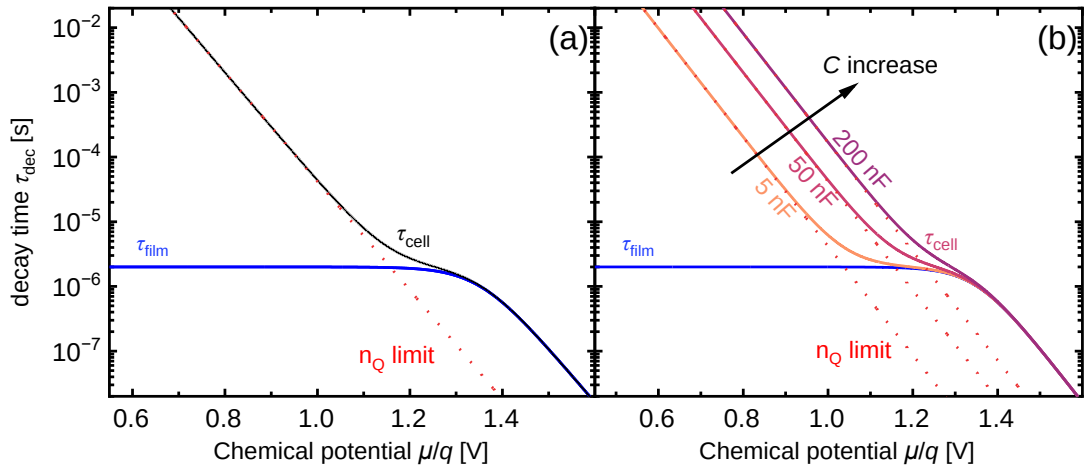

Figure 4.1: Illustration of (a) decay time versus the chemical potential calculated from analytical solutions and (b) decay time versus the chemical potential with the variation of the capacitance (5 nF, 50 nF, 200 nF).

In Figure 4.1(a), the decay time (in black) on the complete perovskite solar cell shows three regions: long decay times at low chemical potential, short and constant decay at intermediate chemical potential, and fast decay at high chemical potential. The long decay time observed at low chemical potential results from the capacitive discharge effect of the contacts i.e., the recombination of charge carriers is delayed through the need to discharge the capacitance before carriers can recombine. In this case, there are fewer charges in the absorber than in the contacts and the decay time becomes $\tau^{\mathrm{LS}}_{\mathrm{cell,HLI}}(n \ll n_{\mathrm{Q}}) \approx n_{\mathrm{Q}}\tau^{\mathrm{eff}}_{\mathrm{SRH}}/n$, the discharging of the capacitor becomes therefore dominant. Whereby at high chemical potential, the decay time is dominated by radiative recombination. In this situation, the charge carrier density in the absorber is very high compared to that of charges induced on the capacitor ($n \gg n_{\mathrm{Q}}$).The decay time approaches thus $\tau^{\mathrm{LS}}_{\mathrm{cell,HLI}}(n \gg 1/(k_{\mathrm{rad}}\tau^{\mathrm{eff}}_{\mathrm{SRH}}) \approx 1/(k_{\mathrm{rad}}n))$. Radiative recombination leads the process. At intermediate chemical potential ($n_{\mathrm{Q}} < n < 1/(k_{\mathrm{rad}}\tau^{\mathrm{eff}}_{\mathrm{SRH}})$, the decay time is fast and reaches a plateau and becomes relatively constant at $\tau^{\mathrm{eff}}_{\mathrm{SRH}} = 2\mu s$, this short decay is therefore dominated by Shockley-Read-Hall recombination.

After analysis, it clearly appears that the decay time varies with the chemical potential in perovskite solar cells.

In contrast to the variation of the Shockley-Read-Hall recombination lifetime in [14] to show the effect of the lifetime on the decay time, in this work the capacitance was varied. In Figure

4.1(b), the decay time is plotted against the chemical potential by varying the capacitance to show the effect of the capacitance on the shape of the decay time at the relatively low chemical potential. It can be seen that the effect of capacitance (discharging) extends the decay time.

In sum, in addition to the Shockley-Read-Hall recombination and radiative recombination mechanisms occurring in transient photoluminescence of both a pure perovskite film and a complete perovskite solar cell, the capacitive effect occurs in a complete perovskite solar cell which makes more challenging the interpretation of transient photoluminescence. These results are in agreement with those found in [14].

Table 4.1: Parameters used in Figure 4.1.

Parameters	**Units**	**Values**
SRH lifetime $\tau_{\mathrm{SRH}}^{\mathrm{eff}}$	µs	2
Radiative recombination coefficient k_{rad}	$cm^3\ s^{-1}$	5×10^{11}
Capacitance per area C_{area}	$nF\ cm^{-2}$	50
Thickness d	nm	700

4.2 Numerical simulations in perovskite solar cell

To gain insight into the charge carrier mechanisms in the complete perovskite solar cell, the graphs in Figure 4.2 have been plotted to describe the same processes but in different images or approaches.

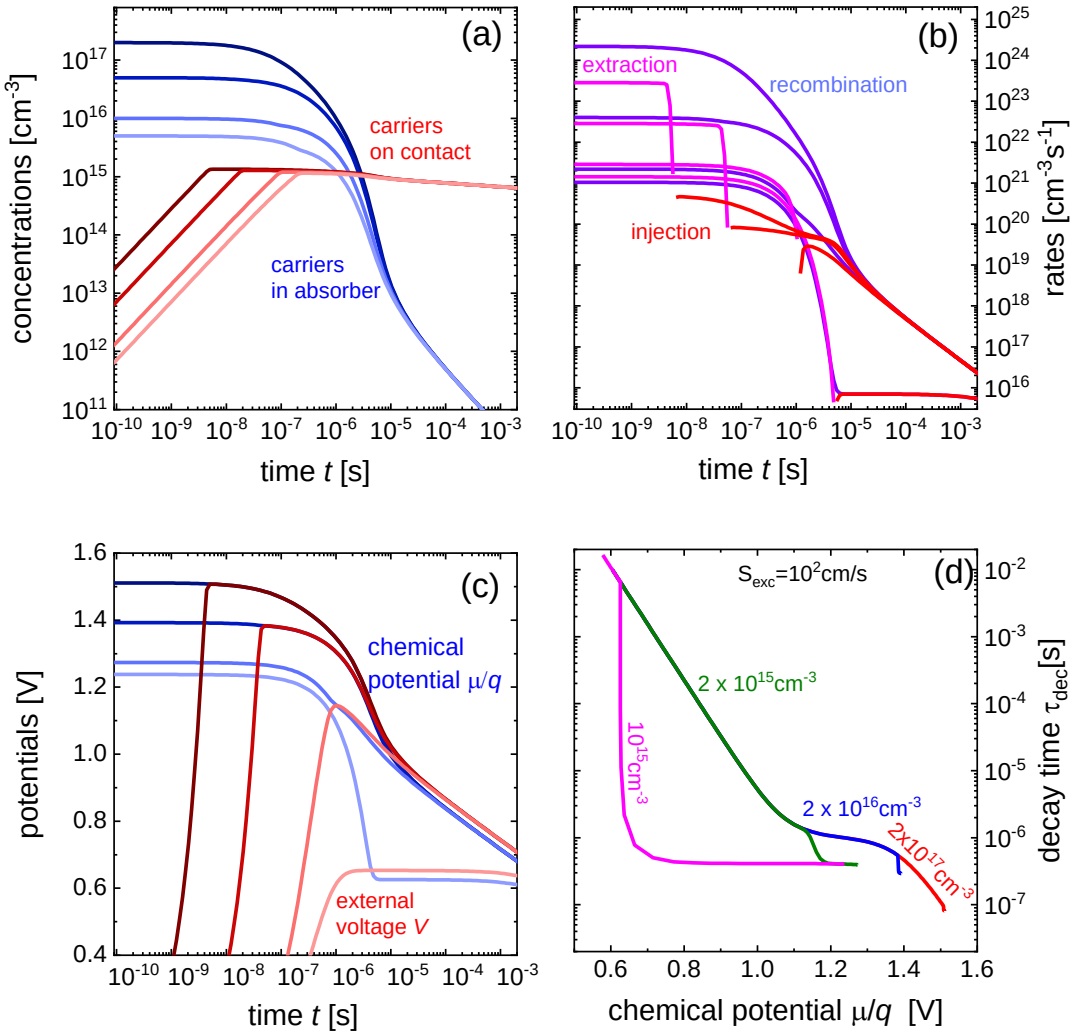

Figure 4.2 (a-d): Illustration of the results of the numerical simulations: (a) charge carriers in the absorber and contacts; (b) extraction, injection, and recombination mechanisms in perovskite solar cells; (c) chemical potential and external voltage in perovskite solar cells over time; (d) decay time against the chemical potential in perovskite solar cell.

Table 4.2: Parameters used in Figure 4.2

Parameters	**unit**	**Value (s)**
SRH lifetime $\tau_{\mathrm{SRH}}^{\mathrm{eff}}$.	µs	1
Exchange velocity S_{exc}	cm/s	100
Radiative recombination coefficient k_{rad}	$\mathrm{cm}^3\ \mathrm{s}^{-1}$	5×10^{11}
Capacitance per area C_{area}	nF cm^{-2}	20
Thickness d	nm	700
Intrinsic carrier concentration n_{i}	cm^{-3}	3.82×10^4
Initial carrier concentration n	cm^{-3}	$2 \times 10^{17}, 2 \times 10^{16}, 10^{16}, 10^{15}$

Figure 4.2 (a) shows charge carrier concentrations in the absorber and on the contacts plotted against the time. The concentration of charge carriers in both the absorber layer (in blue) and the contact layers (in red) over time is illustrated at different initial conditions. From the graph, we have observed that the concentration of charge carriers in the absorber is higher at the early times (right after the excitation by a laser pulse) than the concentration on the contacts. While the concentration of charge carriers in the absorber decreases, the concentration of charges on the contacts increases. However, the concentration of charge carriers in the absorber drops exponentially in the range of 10^{-7} to 10^{-2}s but the density of charges on contacts decreases linearly. Indeed, this charge carrier behavior in a complete perovskite solar cell is explained by the fact that after the excitation of the cell by a laser pulse, charges are created in the absorber layer due to photon absorption and are subsequently extracted from the absorber and transferred to the contacts. As a result, the density of charges in the absorber drops while it increases on the contacts. The exponential decrease of charge carriers in the absorber is explained by the density of charges in the absorber expressed as: $n_{\mathrm{abs}} = n_{\mathrm{i}}\exp(qV_{\mathrm{ext}}/2kT)$ which is exponential dependent. While the slight decrease in the contact is explained by the density of charges on the contact expressed as $n_{\mathrm{c}} = C_{\mathrm{area}}V_{\mathrm{ext}}/qd$ which is linear. In addition, some charges might recombine before reaching the contacts explaining the density drop on the contacts.

Figure 4.2(b) depicts different charge carrier processes involved in a complete perovskite solar cell after excitation by a laser pulse. The graph shows the rate currents plotted over time. Three mechanisms are illustrated on the graph at 4 different initial conditions: the injection (in red),

the extraction (in violet), and the recombination (in blue) of charge carriers. From this figure, one can observe that after the laser excitation, there is the generation of charge carriers in the absorber layer of the cell due to the absorption of photons. Those charge carriers in the absorber are then extracted from the absorber to the contacts therefore the density of charges in the absorber decreases over time. Alternatively, charge carriers injected from the contacts flow back into the absorber i.e., injection of charges, and then the density of charges on contacts decreases. The recombination mechanism is also depicted on the graph alongside the injection and extraction of charge carriers. Some of the charge carriers recombine before reaching the contacts resulting in a decrease in charge carrier injection and extraction density. Furthermore, at the lowest charge carrier density, there is a low charge injection back to the absorber and this happens with a delay. Indeed, at high initial conditions (high light intensity), in this case $2 \times 10^{17}\mathrm{cm}^{-3}$, recombination of carriers dominates over extraction, whereas at relatively low light intensities extraction dominates. The extraction and injection of carriers are controlled by the exchange current density J_{exc}, expressed in Eq. 3.1. A positive value of J_{exc} favors the extraction of charges from the absorber to the contacts, while charges injected from the contacts flow back into the absorber when J_{exc} is negative. The extraction and injection of charge carriers in perovskite solar cell do not occur at the same time.

Figure 4.2(c) illustrates the different potential trends i.e., the chemical potential (Fermi-level splitting or internal voltage) and the external voltage in perovskite solar cells after a laser pulse at four different initial conditions. The chemical potential (in blue) and the external voltage (in red) are plotted over time. From 10^{-10} to 10^{-9}s, the chemical potential is built up and constant in the solar cell at different initial conditions while the external voltage is zero. After some nanoseconds, the external voltage builds up and rises to attain its maximum value for the first 3 initial conditions, $2 \times 10^{17}\mathrm{cm}^{-3}, 10^{16}\mathrm{cm}^{-3}$, and $2 \times 10^{15}\mathrm{cm}^{-3}$ respectively at 1ns, 15 ns and 120 ns with $V_{\mathrm{ext}} = \mu/q$. The external voltage corresponding to the lowest charge density i.e., $10^{15}\mathrm{cm}^{-3}$ needs around 300 ns to build up and attain its maximum value. Subsequently, both the chemical potential and the external voltage decrease exponentially except the external voltage and chemical voltage corresponding to $10^{15}\mathrm{cm}^{-3}$ that remain constant from 5×10^{-6}s. However, the decays of the chemical voltage and external voltage do not overlap. From this graph it can be observed that while the chemical potential is built up and is present inside the cell immediately after excitation, the external voltage takes time (in the order of nanoseconds) to build up and reach its maximum value. This can be explained by the fact that the decay of the chemical potential and the external voltage at a relatively high charge density is limited by

recombination, whereas this decay is limited by extraction at a relatively low charge density. Furthermore, the point at which the external and chemical potentials are equal (maximum value for the external voltage) constitutes the transition point from extraction to injection of carriers in the perovskite solar cell. To see the trend of the chemical potential and the external voltage in a different way, the external voltage is plotted against the chemical potential and shown in Figure A1(b) in the Appendix. The graph shows the same trend as observed in Figure 4.2(c) with the transition point between the extraction and injection of charges.

Furthermore, the decay time against the chemical potential in perovskite solar cell is presented in Figure 4.2(d) at 4 different initial conditions, investigating the power input dependence of the decay time. This graph depicts longer decay times at low chemical potential. This decay time at low chemical potential rises to values above 10^{-2}s while at intermediate chemical potential, it shows the expected Shockley-Read-Hall lifetime at the inflection point. At high chemical potential, the decay time is fast and dominated by the radiative process. This decay time shows the same trend as observed in the analytical solutions with one exception at relatively low initial carrier density of $10^{15}\mathrm{cm}^{-3}$with a different shape of the decay time. The decay time at initial charge carrier densities of $10^{15}\mathrm{cm}^{-3}$ is very long at a very low chemical potential and then shows a flat initial lifetime plateau at intermediate chemical potential, a characteristic of the decay time that is not seen from analytical solutions. It is important to note that the numerical simulations consider the S_{exc}, the velocity at which charge carriers move from the absorber to the contacts and vice versa while the analytical solutions do not. Therefore, from the numerical simulations, the initial lifetime plateau is visible for relatively low fluence through the S_{exc}. The upper curve corresponding to higher light intensities (2×10^{17} cm^{-3}, 2×10^{16} cm^{-3}, 10^{16} cm^{-3}) with the asymptotic behavior gives more information about the material properties while the lower curve corresponding to the lowest light intensity (10^{15} cm^{-3}) gives the combination of the extraction of charge carriers and the lifetime. The same trend of the decay time at different initial conditions is illustrated in Figure A1(a) in the Appendix where the decay time is plotted over time.

4.2.1 Determination of the rise lifetime in perovskite solar cells

Figure 4.3 shows the decay time plotted against the chemical potential as discussed earlier. However, the focus here is to explain how to extract the decay lifetime constant τ^{LS} (grey curve) in perovskite solar cell in large signal.

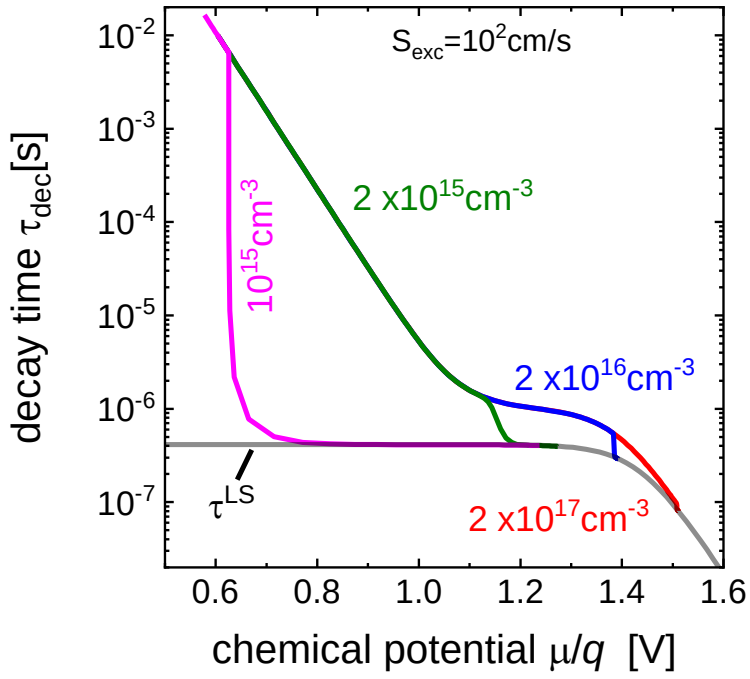

Figure 4.3: Illustration of the decay time against the chemical potential.

To determine this lifetime constant for the rise, we used Eq 3.1,

$$\frac{dn(t)}{dt} = -k_{\mathrm{rad}}(n(t)^2 - n_0^2) - \frac{(n(t)-n_0)}{\tau_{\mathrm{SRH}}^{\mathrm{eff}}} - \frac{S_{\mathrm{exc}}}{d}\left(n(t) - n_0 \exp\left(\frac{qV_{\mathrm{ext}}}{2kT}\right)\right).$$

Since $\tau^{\mathrm{LS}} = -\frac{n(t)}{dn(t)/dt}$, $\tau^{\mathrm{LS}} = -\frac{n(t)}{-k_{\mathrm{rad}}(n(t)^2-n_0^2)-(n(t)-n_0)/\tau_{\mathrm{SRH}}^{\mathrm{eff}}-S_{\mathrm{exc}}/d(n(t)-n_0\exp(qV_{\mathrm{ext}}/2kT))}$.

With assumption $n_0 \ll n(t)$ at t=0, $\tau^{\mathrm{LS}} = \frac{1}{1/\tau_{\mathrm{SRH}}^{\mathrm{eff}} + k_{\mathrm{rad}}n(0)+S_{\mathrm{exc}}/d - n_0 S_{\mathrm{exc}} \exp(qV_{\mathrm{ext}}/2kT)/n(0)\, d}$.

With $n_0/n(0) \ll 1$, we further assume that $S_{\mathrm{exc}}/d \gg n_0 S_{\mathrm{exc}} \exp(qV_{\mathrm{ext}}/2kT)/n(0)\, d$,

$$\tau^{\mathrm{LS}} = \left(\frac{1}{\tau_{\mathrm{SRH}}^{\mathrm{eff}}} + k_{\mathrm{rad}}n + \frac{S_{\mathrm{exc}}}{d}\right)^{-1}.$$

This is the plotted constant rise lifetime for the rise illustrated in Figure 4.3. τ^{LS} represents the extraction and recombination approximation. τ^{LS} is a parallel connection of Shockley-Read-Hall recombination, radiative recombination, and the time constant d/S_{exc} for the rise and decay of charges in the absorber.

4.3 Experimental Results

This section presents the results of the measurements of transient photoluminescence described in section 3 to get insight into different mechanisms involved in a perovskite solar cell. Figure 4.4 illustrates these results.

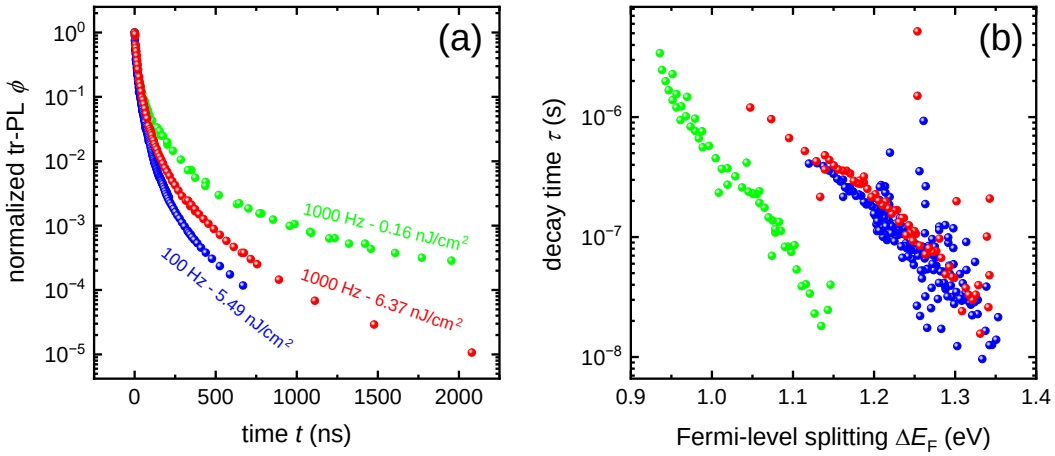

Figure 4.4: Illustration of (a) normalized photoluminescence transients of the perovskite solar cell for different excitation fluences and (b) the decay time over the Fermi-level splitting.

Figure 4.4(a) shows the normalized PL at three different excitation fluences. The plot shows a mono-exponential long-term photoluminescence decay at early delay times and a single exponential decay for each fluence at longer delay times. The mono-exponential long-term photoluminescence decays correspond to Shockley-Read-Hall, while the single exponential decay corresponds to radiative recombination. From Figure 4.4(a), it is observed that the higher the fluence, the faster the photoluminescence decay. Understanding the charge carrier mechanisms in perovskite solar cells therefore requires the application of different light intensities to the cell.

Figure 4.4(b) shows the decay of a perovskite solar cell at three different initial conditions. The decay corresponding to $5.49\ \mathrm{nJ/cm^{-2}}$ light intensity shows three different regions as discussed earlier in the numerical simulations, while the two other decays corresponding to two other initial conditions show only an asymptotic decay. This result might be due to the properties of the perovskite cell used. The performance of the perovskite solar cell used for the measurement is illustrated in Figure A2 in the Appendix.

4.4 Comparison of the Model with SETFOS Software

To further investigate influences such as diffusion and possible inequality of *n* and *p*, we used SETFOS software to compare the results of numerical simulations. SETFOS is used to analyze, model, and simulate the behavior of solar cell devices including their optical and electrical properties, by solving the full rate equations including the possibility of mobile ions.

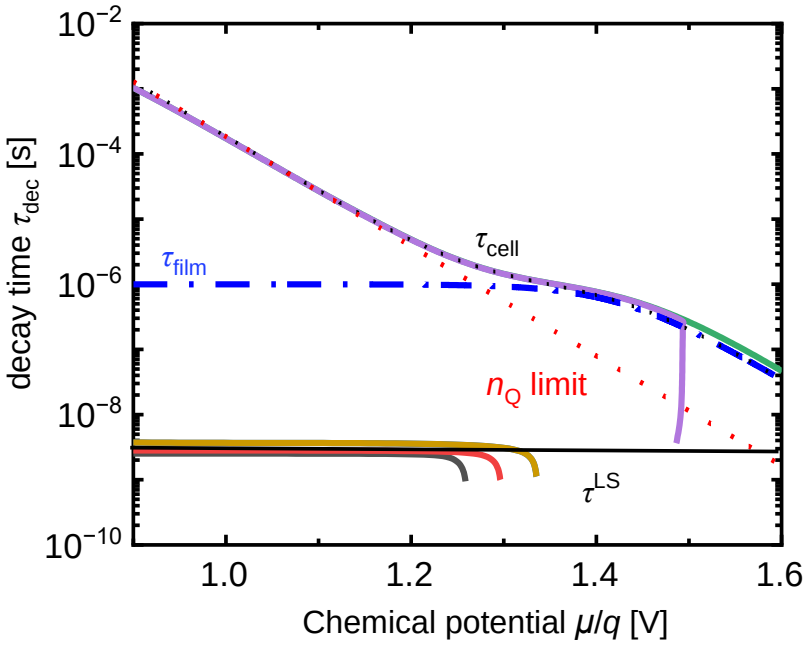

Figure 4.5: Illustration of the decay time against the chemical potential. Simulations obtained by SETFOS.

In Figure 4.5, the decay time of perovskite pure film (in blue) and a perovskite solar cell at different initial conditions is plotted over the chemical potential.

The decay time curve of the film shows two distinct regions, as previously discussed in the numerical simulations: the region of constant decay time at low chemical potential, dominated by Shockley-Read-Hall recombination, and the region of radiative decay.

The decay time of the perovskite cell shows three regions for relatively high initial conditions (green and violet curves): long decay times at very low chemical potential, fast and constant decay at higher chemical potential, and the region of radiative recombination. The decay time at low initial conditions shows two regions as shown in the numerical simulations. The results from the model developed by numerical solutions confirm and validate the results by SETFOS.

5. Conclusion and Outlook

The aim of this work is to numerically simulate the photoluminescence transients in a complete perovskite solar cell to account for the influence of contact capacitance, i.e., charging and discharging effects on photoluminescence, and different carrier mechanisms. It also aimed to gain insight into the recombination, injection and extraction of carriers in perovskite solar cells.

The simulations of photoluminescence transients in perovskite solar cells performed in this work have provided valuable insights into the kinetics of charge carriers in time domain measurements. Through the numerical simulations, we successfully revealed different features of the dynamics of the carrier decay time in a complete perovskite solar cell in response to a laser pulse. Furthermore, we were able to understand and explain the extraction, injection and recombination of carriers after a laser pulse in a complete perovskite solar cell. In addition, the work has explained the difference between the external voltage and the chemical potential and how these two quantities change after a laser pulse in a complete perovskite solar cell. Finally, we were able to extract the time constant for the rise and decay of charge carriers in a complete perovskite solar cell in photoluminescence transients. In summary, the work has provided a method to use analytical and numerical solutions to systems of differential equations in a complete perovskite solar cell to extract information about the decay of transient photoluminescence. This work has contributed to a better understanding of the different charge carrier mechanisms involved in a complete perovskite solar cell.

Future perspectives

In simulating photoluminescence transients in perovskite solar cells in this work, we have only considered a deep defect, i.e., located in the middle of the band gap of the perovskite solar cell. Future work should also consider shallow defects close to the conduction band on one hand and the valence band on the other hand, in order to take into account, the influence of the defect position on the photoluminescence transients in perovskite solar cells, while maintaining the assumptions made so far. In addition, future studies should consider two different defects, shallow and midgap defects for instance, at different levels in the cell to gain more insight into the photoluminescence transient behavior. moreover, careful experiments should be conducted in order to see how the decay time looks like at relatively low fluence.

In addition, future works should focus on developing a mathematical matrix model to determine the rise time τ^{LS} using Taylor expansion.

Bibliography

[1] United Nations Population Division, "The World at Six Billion," *United Nations Publ.*, pp. 1–63, 1999.

[2] P. Gerland *et al.*, "World population stabilization unlikely this century," *Science.*, vol. 346, no. 6206, pp. 234–237, 2014, doi: 10.1126/science.1257469.

[3] A. M. Khan and M. Osińska, "How to predict energy consumption in brics countries?," *Energies*, vol. 14, no. 10, pp. 1–21, 2021, doi: 10.3390/en14102749.

[4] T. Ahmad and D. Zhang, "A critical review of comparative global historical energy consumption and future demand: The story told so far," *Energy Reports*, vol. 6, pp. 1973–1991, 2020, doi: 10.1016/j.egyr.2020.07.020.

[5] International Energy Agency, "Global Energy Review : CO2 Emissions in 2021 Global emissions rebound sharply to highest ever level," 2021.

[6] K. Sagna, Y. Lare, and K. Napo, "Sizing of a Photovoltaic Installation for the Needs of an International Airport: Case Study of GNASSINGBE EYADEMA International Airport (AIGE)," *Int. J. Sustain. Green Energy*, vol. 10, no. 3, p. 99, 2021, doi: 10.11648/j.ijrse.20211003.13.

[7] P. G. V. Sampaio and M. O. A. González, "Photovoltaic solar energy: Conceptual framework," *Renew. Sustain. Energy Rev.*, vol. 74, pp. 590–601, 2017, doi: 10.1016/j.rser.2017.02.081.

[8] C. M. Wolff *et al.*, "Orders of Recombination in Complete Perovskite Solar Cells – Linking Time-Resolved and Steady-State Measurements," *Adv. Energy Mater.*, vol. 11, no. 45, Dec. 2021, doi: 10.1002/aenm.202101823.

[9] M. J. P. Alcocer, T. Leijtens, L. M. Herz, A. Petrozza, and H. J. Snaith, "Electron-Hole Diffusion Lengths Exceeding Trihalide Perovskite Absorber," *Science.*, vol. 342, no. 6156, pp. 341–344, 2013, doi: 10.1126/science.1243982.

[10] L. M. Herz, "Charge-Carrier Dynamics in Organic-Inorganic Metal Halide Perovskites," *Annu. Rev. Phys. Chem.*, vol. 67, pp. 65–89, 2016, doi: 10.1146/annurev-physchem-040215-112222.

[11] L. Krückemeier, Z. Liu, T. Kirchartz, and U. Rau, "Quantifying Charge Extraction and Recombination Using the Rise and Decay of the Transient Photovoltage of Perovskite

Solar Cells," pp. 1–20, 2023.

[12] S. Rai, B. K. Pandey, and D. K. Dwivedi, "Device simulation of low cost HTM free perovskite solar cell based on TiO_2 electron transport layer," *AIP Conf. Proc.*, vol. 2220, no. 1, pp. 1–7, 2020, doi: 10.1063/5.0001230.

[13] N. Espinosa, R. García-Valverde, A. Urbina, and F. C. Krebs, "A life cycle analysis of polymer solar cell modules prepared using roll-to-roll methods under ambient conditions," *Sol. Energy Mater. Sol. Cells*, vol. 95, no. 5, pp. 1293–1302, 2011, doi: 10.1016/j.solmat.2010.08.020.

[14] L. Krückemeier, B. Krogmeier, Z. Liu, U. Rau, and T. Kirchartz, "Understanding Transient Photoluminescence in Halide Perovskite Layer Stacks and Solar Cells," vol. 11, no. 19, 2021, doi: 10.1002/aenm.202003489.

[15] Y. Yuan et al., "Shallow Defects and Ultralong Photoluminescence Decay Times up to 280 μs in Triple-Cation Perovskites" 2023.

[16] S. D. Stranks and H. J. Snaith, "Metal-halide perovskites for photovoltaic and light-emitting devices," *Nat. Nanotechnol.*, vol. 10, no. 5, pp. 391–402, 2015, doi: 10.1038/nnano.2015.90.

[17] W. Li, Z. Wang, F. Deschler, S. Gao, R. H. Friend, and A. K. Cheetham, "Chemically diverse and multifunctional hybrid organic-inorganic perovskites," *Nat. Rev. Mater.*, vol. 2, no. 3, 2017, doi: 10.1038/natrevmats.2016.99.

[18] S. C. Tidrow, "Mapping comparison of Goldschmidt's tolerance factor with perovskite structural conditions," *Ferroelectrics*, vol. 470, no. 1, pp. 13–27, 2014, doi: 10.1080/00150193.2014.922372.

[19] F. Staub, "Time-Resolved Photoluminescence on Perovskite Absorber Materials for Photovoltaic Applications.",Ph.D. thesis,University of Duisburg-Essen, pp. 1–213, 2020.

[20] D. Weber, "CH 3 NH 3 PbX 3 , a Pb(II)-System with cubic perovskite structure," vol. 1445, no. 12, pp. 1443–1445, 1978.

[21] D. B. Mitzi, S. Wang, C. A. Feild, C. A. Chess, and A. M. Guloy, "Conducting layered organic-inorganic halides containing 〈110〉-oriented perovskite sheets," *Science.*, vol. 267, no. 5203, pp. 1473–1476, 1995, doi: 10.1126/science.267.5203.1473.

[22] D. Mitzi, C. Feild, W. Harrison, and A. Guloy, “Conducting tin halides with a layered organic,” *Nature*, vol. 369, no. 6480, pp. 467–469, 1994.

[23] A. Kojima, K. Teshima, Y. Shirai, and T. Miyasaka, “Organometal halide perovskites as visible-light sensitizers for photovoltaic cells,” *J. Am. Chem. Soc.*, vol. 131, no. 17, pp. 6050–6051, 2009, doi: 10.1021/ja809598r.

[24] Lee, M. M., Teuscher, J., Miyasaka, T., Murakami, T. N., & Snaith, H. J., “Efficient hybrid solar cells based on meso-superstructured organometal halide perovskites,” *Science*, vol. 338, no. 6107, pp. 643–648, 2012.

[25] H. Kim *et al.*, “ Lead Iodide Perovskite Sensitized All-Solid-State Submicron Thin Film Mesoscopic Solar Cell with Efficiency Exceeding 9%,” pp. 1–7, 2012, doi: 10.1038/srep00591.

[26] National Renewable Energy Laboratory,“Best Research-Cell Efficiencies,”, 2020.

[27] S. K. Pathak *et al.*, “Performance and Stability Enhancement of Dye-Sensitized and Perovskite Solar Cells by Al Doping of TiO_2,” *Adv. Funct. Mater.*, vol. 24, no. 38, pp. 6046–6055, 2014, doi: 10.1002/adfm.201401658.

[28] Q. Jiang, X. Zhang, and J. You, “SnO_2: A Wonderful Electron Transport Layer for Perovskite Solar Cells,” *Small*, vol. 14, no. 31, pp. 1–14, 2018, doi: 10.1002/smll.201801154.

[29] T. Lemercier, L. Perrin, E. Planès, S. Berson, and L. Flandin, “A Comparison of the Structure and Properties of Opaque and Semi-Transparent NIP/PIN Type Scalable Perovskite Solar Cells,” *Energies*, vol. 13, no. 15, pp. 1–18, 2020, doi: 10.3390/en13153794.

[30] W. S. Yang *et al.*, “Iodide management in formamidinium-lead-halide-based perovskite layers for efficient solar cells,” *Science.*, vol. 356, no. 6345, pp. 1376–1379, 2017, doi: 10.1126/science.aan2301.

[31] M. A. Green, E. D. Dunlop, J. Hohl-Ebinger, M. Yoshita, N. Kopidakis, and A. W. Y. Ho-Baillie, “Solar cell efficiency tables (Version 55),” *Prog. Photovoltaics Res. Appl.*, vol. 28, no. 1, pp. 3–15, 2020, doi: 10.1002/pip.3228.

[32] D. Luo *et al.*, “Enhanced photovoltage for inverted planar heterojunction perovskite solar cells,” *Science.*, vol. 360, no. 6396, pp. 1442–1446, 2018, doi:

10.1126/science.aap9282.

[33] M. Yuan *et al.*, “Perovskite energy funnels for efficient light-emitting diodes,” *Nat. Nanotechnol.*, vol. 11, no. 10, pp. 872–877, 2016, doi: 10.1038/nnano.2016.110.

[34] D. Grabowski, “Photoluminescence-Based Characterization of Charge Extraction and Recombination in Halide-Perovskite Based Solar Cells,” Ph.D. thesis,University of Duisburg-Essen, pp 1–240, 2020.

[35] T. Kirchartz, J. A. Márquez, M. Stolterfoht, and T. Unold, “Photoluminescence-Based Characterization of Halide Perovskites for Photovoltaics,” vol. 1904134, no. 26, 2020, doi: 10.1002/aenm.201904134.

[36] L. Krückemeier, Z. Liu, B. Krogmeier, U. Rau, and T. Kirchartz, “Consistent Interpretation of Electrical and Optical Transients in Halide Perovskite Layers and Solar Cells,” vol. 2102290, no. 46, 2021, doi: 10.1002/aenm.202102290.

[37] V. Sarritzu *et al.*, “Optical determination of Shockley-Read-Hall and interface recombination currents in hybrid perovskites,” *Sci. Rep.*, vol. 7, no. 1, pp. 1–10, 2017, doi: 10.1038/srep44629.

[38] M. Stolterfoht *et al.*, “Visualization and suppression of interfacial recombination for high-efficiency large-area pin perovskite solar cells,” *Nat. Energy*, vol. 3, no. 10, pp. 847–854, 2018, doi: 10.1038/s41560-018-0219-8.

[39] S. Sharma, K. K. Jain, and A. Sharma, “Solar Cells: In Research and Applications—A Review,” *Mater. Sci. Appl.*, vol. 06, no. 12, pp. 1145–1155, 2015, doi: 10.4236/msa.2015.612113.

[40] Y. Xu, T. Gong, and J. N. Munday, “The generalized Shockley-Queisser limit for nanostructured solar cells,” *Sci. Rep.*, vol. 5, no. 1, pp. 1–9, 2015, doi: 10.1038/srep13536.

[41] J. F. Guillemoles, T. Kirchartz, D. Cahen, and U. Rau, “Guide for the perplexed to the Shockley–Queisser model for solar cells,” *Nat. Photonics*, vol. 13, no. 8, pp. 501–505, 2019, doi: 10.1038/s41566-019-0479-2.

[42] O. D. Miller, E. Yablonovitch, and S. R. Kurtz, “Strong internal and external luminescence as solar cells approach the Shockley-Queisser limit,” *IEEE J. Photovoltaics*, vol. 2, no. 3, pp. 303–311, 2012, doi: 10.1109/JPHOTOV.2012.2198434.

[43] B. M. Soucase, I. Guaita Pradas, and K. R. Adhikari, “Numerical Simulations on Perovskite Photovoltaic Devices,” *Perovskite Mater. - Synth. Characterisation, Prop. Appl.*, 2016, doi: 10.5772/61751.

[44] M. R. A. Elsayed, A. M. Elseman, A. A. Abdelmageed, H. M. Hashem, and A. Hassen, “Synthesis and numerical simulation of formamidinium-based perovskite solar cells: a predictable device performance at NIS-Egypt,” *Sci. Rep.*, vol. 13, no. 1, pp. 1–16, 2023, doi: 10.1038/s41598-023-37018-y.

[45] T. Minemoto, M. Murata, H. J. Du, W. C. Wang, Y. F. Gu, and L. C. Slm, “Numerical Simulation and Performance Optimization of,” *Chinese Phys. B*, vol. 116, no. 2, pp. 1–65, 2017.

[46] G. Krishna Burra, D. Sundar Ghosh, S. Tiwari, and Bg. Krishna, “Device Simulation of Perovskite/Silicon Tandem Solar Cell with Antireflective Coating,” 2021, Available: https://doi.org/10.21203/rs.3.rs-790945/v1

[47] Z. Liu *et al.*, “Open-Circuit Voltages Exceeding 1.26 v in Planar Methylammonium Lead Iodide Perovskite Solar Cells,” *ACS Energy Lett.*, vol. 4, no. 1, pp. 110–117, 2019, doi: 10.1021/acsenergylett.8b01906.

A. Appendix

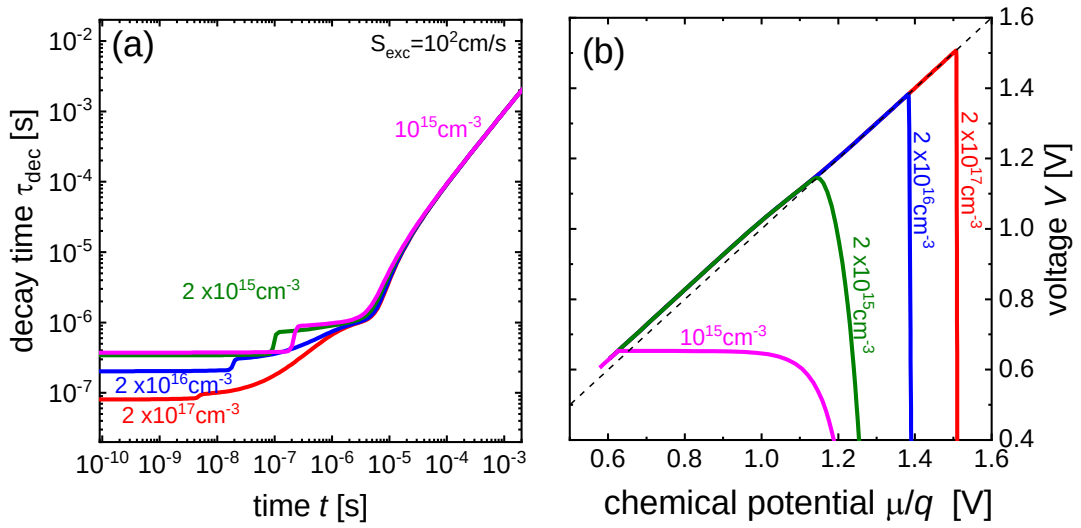

Figure A.1: Illustration of the (a) chemical potential and external voltage in perovskite solar cells (b) decay time against the time and chemical potential in perovskite solar cell.

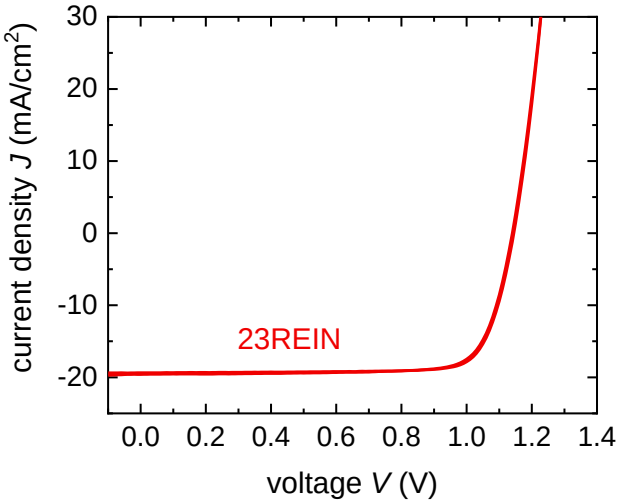

Figure A.2: Illustration of the current-voltage curve of the device used in the measurement.